

# Hilbert Curve Projection Distance for Distribution Comparison

Tao Li

Institute of Statistics and Big Data, Renmin University of China, Beijing, China  
20190001531t@ruc.edu.cn

Cheng Meng\*

Institute of Statistics and Big Data, Renmin University of China, Beijing, China  
chengmeng@ruc.edu.cn

Jun Yu

School of Mathematics and Statistics, Beijing Institute of Technology, Beijing, China  
yujunbeta@bit.edu.cn

Hongteng Xu<sup>†</sup>

Gaoling School of Artificial Intelligence, Renmin University of China, Beijing, China  
hongtengxu@ruc.edu.cn

## Abstract

Distribution comparison plays a central role in many machine learning tasks like data classification and generative modeling. In this study, we propose a novel metric, called *Hilbert curve projection (HCP) distance*, to measure the distance between two probability distributions with high robustness and low complexity. In particular, we first project two high-dimensional probability densities using Hilbert curve to obtain a coupling between them, and then calculate the transport distance between these two densities in the original space, according to the coupling. We show that HCP distance is a proper metric and is well-defined for absolutely continuous probability measures. Furthermore, we demonstrate that the empirical HCP distance converges to its population counterpart at a rate of no more than  $O(n^{-1/2d})$  under regularity conditions. To suppress the curse-of-dimensionality, we also develop two variants of the HCP distance using (learnable) subspace projections. Experiments on both synthetic and real-world data show that our HCP distance works as an effective surrogate of the Wasserstein distance with low complexity and overcomes the drawbacks of the sliced Wasserstein distance.

*Keywords:* Distribution comparison, optimal transport, Hilbert curve, Wasserstein distance, projection robust Wasserstein distance

---

\*Joint first author

<sup>†</sup>Corresponding author

# 1 Introduction

Measuring the distance between two probability distributions is significant for many machine learning tasks, e.g., data classification [22; 16; 37], generative modeling [11; 19], among others. Among the commonly-used distance measures for probability distributions, classic  $f$ -divergence based metrics, e.g., the Kullback-Leibler (KL) divergence and the total variation (TV) distance, do not work well for the probability distributions having disjoint supports [2], while the kernel-based methods like the maximum mean discrepancy (MMD) [12] require sophisticated kernel selection. Recently, the Wasserstein distance [41] has attracted wide attention in the machine learning community because of its advantages on overcoming these limitations, and it has shown great potentials in many challenging learning problems [40; 2; 27].

Given the samples of the two distributions, the computation of Wasserstein distance corresponds to solving either differential equations [8; 4] or linear programming problems [38; 33]. To alleviate the computational burden, the Sinkhorn distance [9] imposes an entropic regularizer on the Wasserstein distance and leverages the Sinkhorn-scaling algorithm accordingly. The work in [2] considers the Kantorovich duality of Wasserstein distance and converts the problem to a “max-min” game. Besides these two approximation methods, more surrogates of the Wasserstein distance are proposed in recent years [43], e.g., the sliced Wasserstein (SW) distance [6], the generalized sliced Wasserstein (GSW) distance [20], the tree-structured Wasserstein (TSW) distance [23], and so on. Despite the computational efficiency, these surrogates may fail to provide effective approximations for the Wasserstein distance. Take the two Gaussian mixture distributions in Figure 1(a) as an example. We keep the source distribution (in purple) unchanged while shifting the central Gaussian component of the target distribution (in orange) vertically with an offset  $\alpha \in [0, 1]$ . For the various distances defined between the two distributions, Figure 1(b) shows their changes to  $\alpha$ . Existing methods often lead to coarse approximations of the Wasserstein distance, whose tendencies w.r.t.  $\alpha$  can even be opposite to the Wasserstein distance. This phenomenon indicates that replacing the Wasserstein distance with these surrogates may lead to sub-optimal, even undesired, results in some learning tasks.

In this study, we propose a novel metric for distribution comparison, called Hilbert curve projection (HCP) distance. In principle, our HCP distance first projects two probability distributions along the Hilbert curve [3] of the sample space and then calculates the coupling based on the projected distributions. Such a Hilbert curve projection works better than linear projections on preserving the structure of the data distribution since the Hilbert curve enjoys the locality-preserving property, i.e., the locality between data points in the high-dimensional space being preserved in the projected one-dimensional space [1; 29]. Our HCP distance provides a new surrogate of the Wasserstein distance, with both efficiency and effectiveness — it performs similarly as the Wasserstein distance does and spends less time than other methods, as shown in Figure 1(b) and 1(c), respectively.

We provide in-depth analysis of the HCP distance, demonstrating that it is a well-defined metric for absolutely continuous probability measures with bounded non-zero supports. Given  $n$  samples in  $d$ -dimensional space, the computational complexity for calculating empirical HCP distance is approximately linear to  $n$ , and this empirical HCP distance converges to its population counterpart at a rate of no more than  $O(n^{-1/2d})$  under regularity conditions. Furthermore, to mitigate the curse-of-dimensionality, we develop two variants of the HCP distance using (learnable) subspace projections. We test the HCP distance and its variants on various machine learning tasks, including data classification and generative modeling, and compare them with state-of-the-art methods. Empirical results support the superior performance of the proposed metrics in both synthetic and real-data settings.

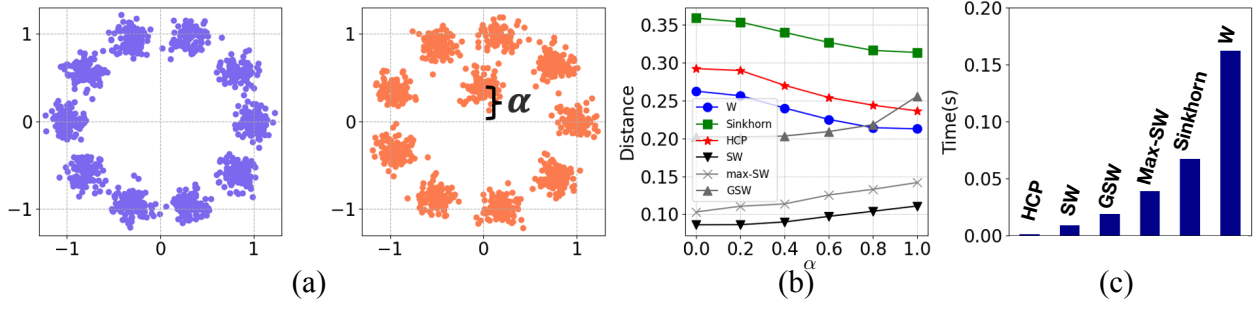


Figure 1: (a) The samples of source and target distributions. (b) Illustrations of various distances with the increase of  $\alpha$ . (c) Comparisons for various distances on their runtime. The proposed HCP distance provides an effective and efficient surrogate of the Wasserstein distance, which performs similarly and has low computational complexity.

## 2 Preliminaries: Wasserstein Distance and Sliced Wasserstein Distance

Let  $(\Omega, d)$  be a metric space and  $\mathcal{P}_p(\Omega)$  be the set of Borel probability measures in  $\Omega$  with finite  $p$ -th moment. Consider two probability measures  $\mu, \nu \in \mathcal{P}_p(\Omega)$  with corresponding probability density functions  $f_\mu, f_\nu$ . The  $p$ -Wasserstein distance [41] between  $\mu$  and  $\nu$  is defined as

$$W_p(\mu, \nu) = \left( \inf_{\gamma \in \Gamma(\mu, \nu)} \int_{\Omega^2} \|x - y\|_p^p d\gamma(x, y) \right)^{1/p} \xrightarrow{\text{1D } \mu, \nu} \left( \int_0^1 \|F_\mu^{-1}(z) - F_\nu^{-1}(z)\|_p^p dz \right)^{1/p} \quad (1)$$

where  $\|\cdot\|_p$  is the  $L_p$  norm and  $\Gamma(\mu, \nu)$  is the set of all couplings (or called transportation plans):

$$\Gamma(\mu, \nu) = \{\gamma \in \mathcal{P}_p(\Omega \times \Omega) \mid \forall \text{ Borel set } A, B \subset \Omega, \gamma(A \times \Omega) = \mu(A), \gamma(\Omega \times B) = \nu(B)\}.$$

Though it is difficult to calculate Wasserstein distance in general, according to Equation (1), for one-dimensional probability measures  $\mu$  and  $\nu$ , the Wasserstein distance has a closed-form, where  $F_\mu(x) = \mu((-\infty, x]) = \int_{-\infty}^x f_\mu(x) dx$  is the cumulative distribution function (CDF) for  $f_\mu$ , and similarly,  $F_\nu$  is the CDF for  $f_\nu$ . This fact motivates the design of the sliced Wasserstein (SW) distance [6] (and its variants [10; 21]), which projects  $d$ -dimensional probability measures to 1D space and computes the 1D Wasserstein distance accordingly. Let  $\mathbb{S}_{d,q} = \{\mathbf{E} \in \mathbb{R}^{d \times q} : \mathbf{E}^\top \mathbf{E} = \mathbf{I}_q\}$  ( $q < d$ ) be the set of orthogonal matrices and  $P_{\mathbf{E}}(\mathbf{x}) = \mathbf{E}^\top \mathbf{x}$  be the linear transformation for  $\mathbf{x} \in \mathbb{R}^d$ . Denote  $P_{\mathbf{E}\#}\mu$  as the pushforward of  $\mu$  by  $P_{\mathbf{E}}$ , which corresponds to the distribution of the projected samples. For all  $\mu, \nu \in \mathcal{P}_p(\Omega)$ , the  $p$ -sliced Wasserstein distance between them is given by

$$SW_p(\mu, \nu) = \left( \int_{\mathbf{E} \in \mathbb{S}_{d,1}} W_p^p(P_{\mathbf{E}\#}\mu, P_{\mathbf{E}\#}\nu) d\sigma(\mathbf{E}) \right)^{1/p}, \quad (2)$$

where  $\sigma$  is the uniform distribution on  $\mathbb{S}_{d,1}$ . However, as aforementioned, the SW distance often fails to approximate the Wasserstein distance because its linear projections break the structure of the original distributions. Additionally, the random projections introduce unnecessary randomness when computing the distance. To overcome the above issues, we propose the HCP distance shown below.

## 3 Proposed Method

### 3.1 Hilbert curve and its locality-preserving property

Our work is based on the well-known Hilbert curve [3]. Mathematically, for a  $d$ -dimensional ( $d \geq 2$ ) unit hyper-cube, i.e.,  $[0, 1]^d$ , the  $k$ -order Hilbert space-filling curve, denoted as  $\hat{H}_k$ , partitions  $[0, 1]$

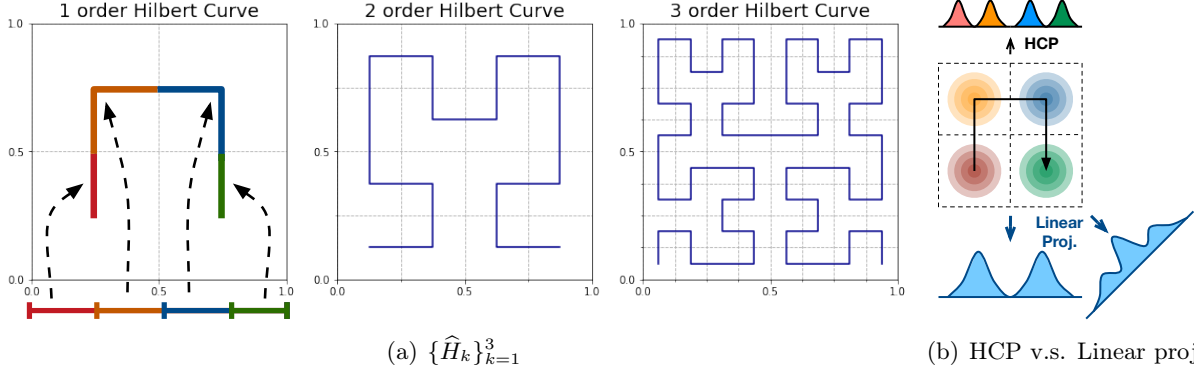


Figure 2: (a) The  $k$ -order Hilbert curve, with  $k = 1, 2, 3$ , in 2D space. (b) The comparison between Hilbert curve projection (HCP) and linear projections.

and  $[0, 1]^d$  into  $(2^k)^d$  intervals and blocks, respectively, and constructs a bijection between them. Taking the  $\{\hat{H}_k\}_{k=1}^3$  in 2D space as examples, Figure 2(a) illustrates how the intervals in  $[0, 1]$  are constructed and mapped to the blocks in  $[0, 1]^2$ . The Hilbert curve is defined as the limit of a sequence of  $k$ -order Hilbert space-filling curves, i.e.,  $H(x) = \lim_{k \rightarrow \infty} \hat{H}_k(x)$  with  $x \in [0, 1]$ . It provides a well-defined surjection  $H : [0, 1] \rightarrow [0, 1]^d$  and is able to cover the entire hyper-cube [3]. Note that, although the Hilbert curve  $H$  is not a bijection, most of the data points in  $[0, 1]^d$  are still invertible — it is known that the set  $\mathcal{A}$ , which includes the points in  $[0, 1]^d$  such that these points have more than one pre-image in  $[0, 1]$ , has measure zero [14].

We are interested in the Hilbert curve because it enjoys the so-called **locality-preserving property** [44; 14]: For any  $x, y \in [0, 1]$ , one has  $\|H(x) - H(y)\| \leq 2\sqrt{d+3}|x - y|^{1/d}$ . Such an inequality indicates the advantage of the Hilbert curve over linear projections. In particular, if two points are far from each other in a high-dimensional space, their pre-images with respect to the Hilbert curve will also be far from each other. Figure 2(b) further illustrates this property through a toy example. Specifically, for a 2D distribution with four modals, while linear projections tend to wrongly merge some modals, the projection along the Hilbert curve can distinguish the modals successfully. This property motivates us to propose the Hilbert curve projection distance shown below.

### 3.2 Hilbert curve projection distance

In this study, we focus on absolutely continuous probability measures whose probability density functions have bounded non-zero supports. Denote such a probability measure as  $\mu$ , its corresponding probability density function as  $f_\mu$ , and the support as  $\Omega_\mu$ . For each  $\mu$ , we can define a Hilbert curve as  $H_\mu : [0, 1] \rightarrow \tilde{\Omega}_\mu$ , where  $\tilde{\Omega}_\mu$  is the smallest hyper-rectangle that cover  $\Omega_\mu$ .<sup>1</sup> Let  $X$  be the  $d$ -dimensional ( $d \geq 2$ ) random variable with the probability measure  $\mu$ . According to [44; 14], the Hilbert curve  $H_\mu$  satisfies  $\int_{\mathbf{x} \in \Omega_\mu} f_\mu(\mathbf{x}) d\mathbf{x} = \int_{\mathbf{x} \in \tilde{\Omega}_\mu} f_\mu(\mathbf{x}) d\mathbf{x} = \int_0^1 f_\mu(H_\mu(s)) ds$ . This property motivates us to define a cumulative distribution function along the Hilbert curve (denoted as  $g_\mu : [0, 1] \rightarrow [0, 1]$ ) and the corresponding inverse cumulative distribution function ( $g_\mu^{-1}$ ), respectively:

$$g_\mu(t) = \mu(H_\mu([0, t])) = \int_0^t f_\mu[H_\mu(s)] ds, \quad g_\mu^{-1}(t) = \inf_s \{s \in [0, 1] : g_\mu(s) > t\}. \quad (3)$$

Accordingly, the formal definition of our Hilbert curve projection distance is as follows.

<sup>1</sup>We can extend the range of the Hilbert curve from  $[0, 1]^d$  to  $\tilde{\Omega}_\mu$  simply by linear transformation.

**Definition 1.** Given two absolutely continuous probability measures  $\mu$  and  $\nu$ , whose probability density functions  $f_\mu$  and  $f_\nu$  are defined on bounded supports  $\Omega_\mu$  and  $\Omega_\nu$ , respectively. Let  $H_\mu : [0, 1] \rightarrow \tilde{\Omega}_\mu$ , where  $\tilde{\Omega}_\mu$  is the smallest hyper-rectangle that covers  $\Omega_\mu$ ,  $g_\mu(t) = \mu(H_\mu([0, t])) = \int_0^t f_\mu[H_\mu(s)]ds$ , and  $g_\mu^{-1}(t) = \inf_s \{s \in [0, 1] : g_\mu(s) > t\}$  (with  $H_\nu$ ,  $g_\nu$  and  $g_\nu^{-1}$  defined in the same way). For  $p \in \mathbb{Z}_+$ , the  $p$ -order Hilbert curve projection distance is defined as

$$\text{HCP}_p(\mu, \nu) = \left( \int_0^1 \|H_\mu(g_\mu^{-1}(t)) - H_\nu(g_\nu^{-1}(t))\|_p^p dt \right)^{1/p}. \quad (4)$$

**Remark 1.** Let  $\mathcal{A}_\mu$  be the set that includes the points in  $\tilde{\Omega}_\mu$  such that these points have more than one pre-image in  $[0, 1]$ . Recall that  $\mathcal{A}_\mu$  has measure zero. The constraint that  $f_\mu$  and  $f_\nu$  are absolutely continuous can be relaxed when  $f_\mu$  and  $f_\nu$  are non-degenerate on  $\mathcal{A}_\mu$  and  $\mathcal{A}_\nu$ , respectively.

According to the definition, the principle of our HCP distance is projecting high-dimensional distributions along their Hilbert curves to obtain a coupling between them and then calculating the transport distance between these two densities in the original space. The following theoretical results show that our HCP distance is a proper metric, and the empirical HCP distance (calculated based on samples) converges to its population counterpart at a rate of no more than  $O(n^{-1/2d})$  under mild regularity conditions. The proof is relegated to Supplementary Material.

**Theorem 1.**  $\text{HCP}_p(\mu, \nu)$  is a well-defined metric over all absolutely continuous probability measures in  $\mathcal{P}_p(\Omega)$  and  $W_p(\mu, \nu) \leq \text{HCP}_p(\mu, \nu)$ .

**Theorem 2.** Let  $\mu$  be an absolutely continuous probability measure, whose probability density has bounded non-zero support  $\Omega$  in  $d$ -dimensional space, and  $\mu_n$  is the empirical distribution based on  $n$  samples. Let  $\tilde{\Omega}_\mu = \prod_{i=1}^d [a^{(i)}, b^{(i)}]$  be the smallest hyper-rectangle covering  $\Omega$ . Suppose that (1)  $\Pr(x^{(i)} - a^{(i)} < n^{-1/2}) \leq n^{-1/2}$  and  $\Pr(b^{(i)} - x^{(i)} > n^{-1/2}) \leq n^{-1/2}$  hold for all  $\mathbf{x} = [x^{(i)}]_{i=1, \dots, d} \sim \mu$ ; and (2)  $\int_{s_j - cn^{-1/2}}^{s_j + cn^{-1/2}} f_\mu(H_\mu(s))ds \geq cn^{-1/2}$  holds for every  $\mathbf{x}_j$  corresponding to  $H_{\mu_n}(s_j)$ , where  $j = 1, 2, \dots, n$ , and  $c \in [0, \infty)$ . Then, one has  $n^{-\frac{1}{d}} \lesssim \mathbb{E}[\text{HCP}_p(\mu, \mu_n)] \lesssim n^{-\frac{1}{2d}}$ .

**Corollary 1.** The lower bound shown in Theorem 2 is achievable: If  $\mu$  is uniformly distributed on  $[0, 1]^d$  and the  $n$  sample points lie uniformly on the Hilbert curve, then  $\mathbb{E}[\text{HCP}_p(\mu, \mu_n)] = O(n^{-\frac{1}{d}})$ .

**Remark 2.** One byproduct of Theorem 2 is that it indicates when  $k = O(\log(n))$ , replacing the Hilbert curve with the  $k$ -order Hilbert curve  $\hat{H}_k$  in the HCP distance will not affect its convergence rate; see Supplementary Material for more details.

### 3.3 Numerical implementation

Given the samples of two probability measures, i.e.,  $\{\mathbf{x}_i\}_{i=1}^m \sim \mu$  and  $\{\mathbf{y}_j\}_{j=1}^n \sim \nu$ , whose empirical distributions are  $\mathbf{a} \in \Delta^{m-1}$  and  $\mathbf{b} \in \Delta^{n-1}$ , respectively ( $\Delta^{d-1}$  represents the  $(d-1)$ -Simplex). Let  $\tilde{\Omega}_X$  and  $\tilde{\Omega}_Y$  be the smallest hyper-rectangles that cover these two samples, respectively. We define two  $k$ -order Hilbert curves, i.e.,  $\hat{H}_k^X : [0, 1] \rightarrow \tilde{\Omega}_X$  and  $\hat{H}_k^Y : [0, 1] \rightarrow \tilde{\Omega}_Y$ . Here,  $\hat{H}_k^X$  partitions both  $[0, 1]$  and  $\tilde{\Omega}_X$  into  $2^{kd}$  blocks, denoted by  $\{c'_{j,X}\}_{j=1}^{2^{dk}}$  and  $\{c_{j,X}\}_{j=1}^{2^{dk}}$ , respectively, and construct a bijection between these blocks. For any data point  $\mathbf{x} \in \tilde{\Omega}_X$ , we assign  $\mathbf{x}$  to its corresponding block  $c_{j,X}$  in  $\tilde{\Omega}_X$ ,  $j \in \{1, \dots, 2^{kd}\}$ , then map  $\mathbf{x}$  to the center of the block  $c'_{j,X} = (\hat{H}_k^X)^{-1}(c_{j,X})$ . Therefore, all the samples belonging to the same block are mapped to the same point in  $[0, 1]$ . Based on  $\hat{H}_k^Y$ , we map  $\{\mathbf{y}_j\}_{j=1}^n$  to  $[0, 1]$  in the same way. The mapped points along with their probability densities are then used to calculate the optimal coupling matrix  $\mathbf{P} \in \mathbb{R}^{m \times n}$  using the closed-form formulation

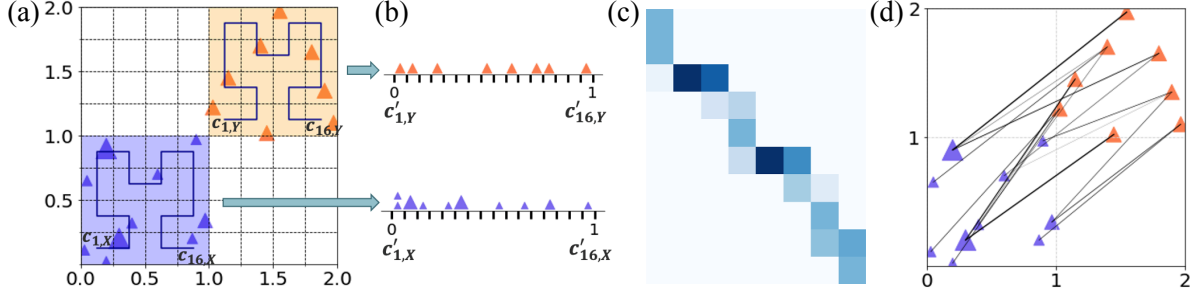


Figure 3: An illustration of Algorithm 1 when  $d = k = 2$ . (a) The source (purple) and target (orange) data points, with corresponding hyper-rectangles and  $k$ -order Hilbert curves. (b) The projected points along the Hilbert curves. (c) The coupling matrix calculated by the projected points. (d) The HCP distance calculates the distance between the original samples based on the coupling matrix.

of the 1D optimal transport problem. In particular, we first sort the mapped points, then calculate  $\mathbf{P}$  using the North-West corner rule with  $O(m + n)$  operations [34]. Note that there are at most  $m + n$  nonzero elements in  $\mathbf{P}$ . Let  $\mathcal{S} := \{(i, j) | P_{ij} \neq 0\}$  be the index set. Finally, the empirical HCP distance then can be calculated by  $(\sum_{(i,j) \in \mathcal{S}} \|\mathbf{x}_i - \mathbf{y}_j\|_p^p P_{ij})^{1/p}$ . The above pipeline is summarized in Algorithm 1 and illustrated in Figure 3. Empirical results show the performance of Algorithm 1 is not sensitive to  $k$ , see Supplementary Material for details.

---

**Algorithm 1** Computation of HCP distance

---

- 1: **Input:**  $(\{\mathbf{x}_i\}_{i=1}^m, \mathbf{a}), (\{\mathbf{y}_i\}_{i=1}^n, \mathbf{b}), k$
  - 2: Map  $\{\mathbf{x}_i\}_{i=1}^m$  to  $\{\mathbf{x}'_i\}_{i=1}^m$ ,  $\{\mathbf{y}_i\}_{i=1}^n$  to  $\{\mathbf{y}'_i\}_{i=1}^n$ , through  $(\hat{H}_k^X)^{-1}$  and  $(\hat{H}_k^Y)^{-1}$   $O((m+n)dk)$
  - 3: Calculate the optimal transport plan  $\mathbf{P}$  between  $(\{\mathbf{x}'_i\}_{i=1}^m, \mathbf{a})$  and  $(\{\mathbf{y}'_i\}_{i=1}^n, \mathbf{b})$  using sorting and the North-West corner rule. Let  $\mathcal{S} := \{(i, j) | P_{ij} \neq 0\}$   $O(m \log(m) + n \log(n))$
  - 4: **Output:**  $\mathbf{P}$ ,  $\text{HCP}_p = (\sum_{(i,j) \in \mathcal{S}} \|\mathbf{x}_i - \mathbf{y}_j\|_p^p P_{ij})^{1/p}$
- 

**Computational cost.** The complexity of computing the  $k$ -order Hilbert index for  $n$  points in  $d$ -dimensional space is  $O(ndk)$  [13; 39; 17]. Solving the optimal transport problem in Step 3 requires  $O(m \log m + n \log n)$  time. When  $m = O(n)$  and  $k = O(\log(n))$  (following Remark 2), the overall computational complexity of Algorithm 1 is at the order of  $O(n \log(n)d)$ .

**Comparison with existing methods.** The proposed HCP distance enjoys several key advantages over the Wasserstein and SW distance. In particular, compared to Wasserstein distance, HCP has an approximately linear computational complexity, and thus is applicable to large-scale datasets. Compared to SW distances, HCP distance performs more similarly as the Wasserstein distance due to the locality-preserving property of the Hilbert curve projection. In addition, HCP distance is able to provide a reasonable coupling matrix between the samples. Such a coupling matrix is essential for effective generative modeling, as will be seen in Section 5. Last but not least, HCP computes faster than SW distance in practice. This is because calculating SW distance requires projection and sorting for a large number of times, while calculating HCP distance requires only once.

Although some work also utilizes Hilbert curve for distribution-free two-sample test [30] and distance measure [5], our HCP distance owns several differences and advantages. Firstly, instead of using a same Hilbert curve [30], we project each probability density separately to corresponding Hilbert curve, which guarantees our HCP distance is a well-defined metric. Secondly, our HCP distance focuses more on the comparison for two probability densities in the original high-dimensional space — given the coupling between the projected densities along Hilbert curves, we go back to the original space to compute distance between the original densities. Finally, beyond the Hilbert

curve-based discrepancy in [5], our HCP distance can deal with the samples with different numbers and weights, whose theoretical properties are guaranteed.

## 4 Variants of the Hilbert Curve Projection Distance

Analogous to the Wasserstein distance, our HCP distance may suffer from the curse-of-dimensionality as well. To overcome this limitation, we propose the following two variants of the HCP distance.

**Integral projection robust Hilbert curve projection distance (IPRHCP distance).** We first propose the IPRHCP distance that combines the idea of HCP distance and random projections.

**Definition 2.** For two absolutely continuous probability measures  $\mu$  and  $\nu$ , whose probability densities  $f_\mu$  and  $f_\nu$  have bounded nonzero supports, their  $p$ -order  $q$ -dimensional integral projection robust Hilbert curve projection distance is defined as

$$IPRHCP_{p,q}(\mu, \nu) = \left( \int_{\mathbf{E} \in \mathbb{S}_{d,q}} HCP_p^p(P_{\mathbf{E}\#}\mu, P_{\mathbf{E}\#}\nu) d\sigma(\mathbf{E}) \right)^{1/p} \quad (5)$$

where  $\sigma$  is the uniform distribution on  $\mathbb{S}_{d,q}$ .

We demonstrate that IPRHCP distance is a valid distance metric and reveal the relations between IPRHCP distance and other metrics, including the  $p$ -order SW distance [6] and the  $p$ -order  $q$ -dimensional integral projection robust Wasserstein distance [26], denoted as  $IPRW_{p,q}$ .

**Proposition 1.**  $IPRHCP_{p,q}(\mu, \nu)$  is a well-defined metric over all absolutely continuous probability measures in  $\mathcal{P}_p(\Omega)$  and  $IPRW_{p,q}(\mu, \nu) \leq IPRHCP_{p,q}(\mu, \nu)$ .

**Proposition 2.**  $SW_p^p(\mu, \nu) \leq \alpha_{q,p} IPRHCP_{p,q}^p(\mu, \nu)$ , where  $\alpha_{q,p} = \int_{\mathbb{S}_{q,1}} \|\theta\|_p^p d\theta / q \leq 1$ . As a special case, when  $p = 2$ , one has  $\alpha_{q,2} = 1/q$  and  $SW_2(\mu, \nu) \leq IPRHCP_{2,q}(\mu, \nu) / \sqrt{q}$ .

**Remark 3.** If we replace  $\mathbb{S}_{d,q}$  in Equation (5) with matrix set  $\{\mathbf{E} \in \mathbb{R}^{d \times q} : \mathbf{E}^\top \mathbf{E} = \mathbf{J}_q\}$  where  $\mathbf{J}_q$  is a  $q \times q$  all-ones matrix, we have  $IPRHCP_{p,q}(\mu, \nu) = q^{1/p} SW_p(\mu, \nu)$ .

In practice, the expectation in Equation (5) can be approximated using a Monte Carlo scheme: We first randomly and uniformly draw several matrices from the set of orthogonal matrices  $\mathbb{S}_{d,q}$ . We then project the distributions to subspace  $\mathbf{E}$  and compute the HCP distance between the projected samples. Finally, we replace the expectation on the right hand side of Equation (5) with a finite-sample average.

**Projection robust Hilbert curve projection distance (PRHCP distance).** The IPRHCP distance considers the integration of the HCP distances defined in all  $q$ -dimensional subspaces. When assuming the two distributions differ only on one low-dimensional subspace, as the projection robust Wasserstein (PRW) distance [25] does, we can avoid the integration and just consider the maximal possible HCP distance among all projections, which leads to the proposed PRHCP distance, i.e.,  $PRHCP_{p,q}(\mu, \nu) := \sup_{\mathbf{E} \in \mathbb{S}_{d,q}} HCP_p(P_{\mathbf{E}\#}\mu, P_{\mathbf{E}\#}\nu)$ .

The PRHCP distance is also a valid distance. In practice, given the samples of the probability measures, i.e., the sample matrices  $\mathbf{X} = [\mathbf{x}_i^\top] \in \mathbb{R}^{m \times d}$  and  $\mathbf{Y} = [\mathbf{y}_i^\top] \in \mathbb{R}^{n \times d}$ , we consider an EM-like optimization scheme to calculate the empirically PRHCP distance, i.e., we optimize the transport plan  $\mathbf{P}$  and the  $d \times q$  orthogonal matrix  $\mathbf{E}$  alternately and iteratively. Details for calculating PRHCP distance are summarized in Algorithm 2. This algorithm is similar to the one for calculating the subspace robust Wasserstein distance in [32], except that the transport plan is calculated by the

---

**Algorithm 2** Computation of PRHCP distance

---

- 1: **Input:**  $(\{\mathbf{x}_i\}_{i=1}^m, \mathbf{a}), (\{\mathbf{y}_i\}_{i=1}^n, \mathbf{b}), k, q$
  - 2: Initialize  $\mathbf{U} = \mathbf{\Omega} = \mathbf{I}_d, t = 0, \tau = 1$
  - 3: **While not converge**
    - a)  $\mathbf{P} \leftarrow \text{Algorithm 1}[(\{\mathbf{U}^\top \mathbf{x}_i\}_{i=1}^m, \mathbf{a}), (\{\mathbf{U}^\top \mathbf{y}_i\}_{i=1}^n, \mathbf{b}), k]$   $O((m \log(m) + n \log(n))d)$
    - b)  $\mathbf{U} \in \mathbb{R}^{d \times q} \leftarrow$  top  $q$  singular vectors of the matrix  $(\text{diag}(\mathbf{a})\mathbf{X} - \mathbf{P}\mathbf{Y})$   $O((m+n)d^2)$
    - c)  $\mathbf{\Omega} \leftarrow (1 - \tau)\mathbf{\Omega} + \tau\mathbf{U}\mathbf{U}^\top$ , and then  $\mathbf{U} \leftarrow$  top  $q$  eigenvectors of  $\mathbf{\Omega}$   $O(d^2q + d^3)$
    - d)  $t \leftarrow t + 1, \tau \leftarrow 2/(2 + t)$
  - 4: **Output:** The coupling  $\mathbf{P}$ , and  $\text{PRHCP}_{p,q} = (\sum_{(i,j) \in \{(i,j) | P_{ij} \neq 0\}} \|\mathbf{U}^\top \mathbf{x}_i - \mathbf{U}^\top \mathbf{y}_j\|_p^p P_{ij})^{1/p}$ .
- 

HCP distance. As shown in Supplementary Material, we find that the convergence trend of our PRHCP distance is very similar to that in projection robust Wasserstein distance [25].

**Computational cost.** For brevity, we consider the case that  $m = n > d > q$ . Step 3(a) requires  $O(n \log(n)d)$  time, as discussed in the last section. Recall that there are at most  $(m+n)$  nonzero elements in  $\mathbf{P}$ , and thus Step 3(b) requires only  $O(m+n)d^2$  time. The cost for Step 3(c) involves  $O(d^2q)$  for  $\mathbf{U}\mathbf{U}^\top$  and  $O(d^3)$  for solving the eigen-decomposition problem, respectively. Thus, the overall complexity of Algorithm 2 is  $O(n \log(n)dL + nd^2L)$ , where  $L$  is the number of iterations.

## 5 Experiments

To demonstrate the feasibility and efficiency of our HCP distance and its variants, we conducted extensive numerical experiments and compared them with the main-stream competitors, including maximum mean discrepancy (MMD), Wasserstein distance, Sinkhorn distance [9], SW distance [6], max-SW distance [10], GSW distance [20], TSW distance [23], and PRW distance [25]. For all the distances, we considered the Euclidean cost, i.e.,  $p = 2$ . We set the dimension for the intrinsic space as  $q = 2$  for PRW, IPRHCP, and PRHCP. All experiments are implemented by a AMD 3600 CPU and a RTX 1080Ti GPU. **Representative experiments are shown below, and more implementation details and results are in Supplementary Material.**

**Approximation of Wasserstein flow.** Following the experiment in [20], we consider the problem  $\min_{\mu} W_2(\mu, \nu)$ , where  $\nu$  is a fixed target distribution, and  $\mu$  is the source distribution initialized as  $\mu_0 = \mathcal{N}(0, 1)$  and updated iteratively via  $\partial_t \mu_t = -\nabla W_2(\mu_t, \nu)$ . We consider two different distributions for the target  $\nu$ , i.e., *25-Gaussians* and *Swiss Roll*, and approximate the Wasserstein distance  $W_2$  by SW, max-SW, GSW, max-GSW, and HCP. Each method applies one projection per iteration and sets the learning rate to be 0.01. The experiments are replicated one hundred times, and we record the averaged 2-Wasserstein distance between  $\mu_t$  and  $\nu$  at each iteration. The comparison for the methods on their convergence curves and the snapshots of their learning results when  $t = 150$  are shown in Figure 4. We can find that applying HCP helps to accelerate the learning process and leads to better results.

**Effectiveness and efficiency for high-dimensional data.** As shown in Figure 1, our HCP distance provides an effective and efficient surrogate of Wasserstein distance for 2D data. Here, we further compare various metrics on approximating Wasserstein distance for high-dimensional data.

In particular, let  $\{\mathbf{x}_i\}_{i=1}^n$  and  $\{\mathbf{y}_i\}_{i=1}^n$  be i.i.d. samples generated from  $\mathcal{N}_d(\mathbf{0}_d, \mathbf{\Sigma}_X)$  and  $\mathcal{N}_d(\mathbf{0}_d, \mathbf{\Sigma}_Y)$ , respectively. We set  $n = 200, d = 50, \mathbf{\Sigma}_X = \text{diag}(3\mathbf{I}_2, \mathbf{I}_{d-2})$  and  $\mathbf{\Sigma}_Y = \text{diag}(3\mathbf{I}_2 + 3\theta\mathbf{B}_2, \mathbf{I}_{d-2})$ , where  $\mathbf{I}_d$  and  $\mathbf{B}_d$  are identity and backward identity matrices with size  $(d \times d)$ , respectively. Given different  $\theta$ 's, we generate different samples and calculate the distance between the two sample sets under different metrics. Figure 5(a) shows the averaged distance in one hundred



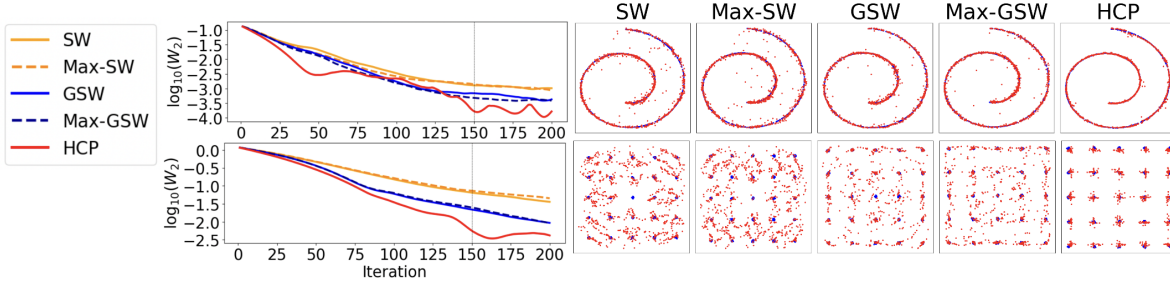


Figure 4: Left: Log 2-Wasserstein distance between the source and target distributions versus the number of iterations  $t$ . Right: A snapshot when  $t = 150$ .

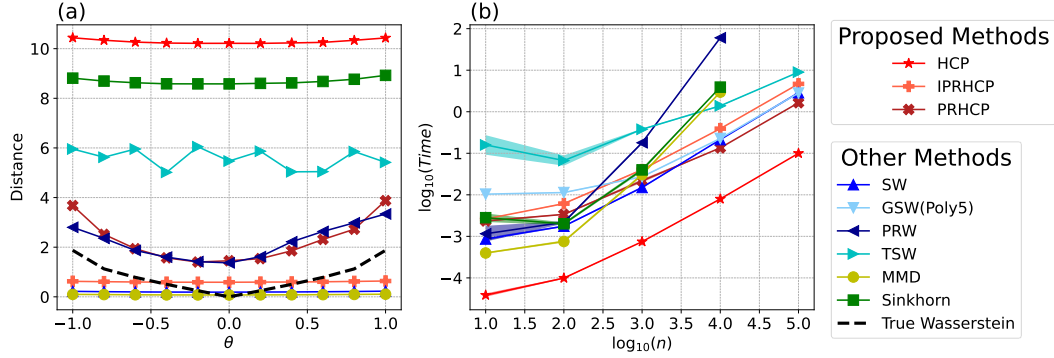


Figure 5: (a) Distances versus different  $\theta$ . (b) CPU time versus different  $n$  when  $d = 4$ .

trials. Taking the true Wasserstein distance between the two Gaussian densities as a benchmark,<sup>2</sup> we observe that most of the metrics considered here suffer from the curse-of-dimensionality, i.e., their distances are not sensitive to the parameter  $\theta$ . Among these methods, the PRW and our PRHCP are the only two that provide reasonable distances — they perform similarly as the true Wasserstein distance, while the latter computes much faster than the former. In the aspect of efficiency, we compare the CPU time for different methods using the aforementioned setting. Figure 5(b) shows the CPU time (in seconds) versus different  $n$ 's. Our HCP requires significantly less time than all the competitors, and its two variants are at least comparable to other distances in runtime. Moreover, the time for our methods, including the HCP distance and its variants, is approximately linear to  $n$ . In summary, the above experimental results validate the potential of the HCP distance and its variants in dealing with large-scale high-dimensional data.

**3D point cloud classification.** For low-dimensional data like 3D points, our HCP distance is superior to other distances in their classification tasks. We consider the ModelNet10 dataset [42] that contains around 5,000 CAD objects from 10 categories. For each category, we randomly sample 50 objects for training and 30 object objects for testing. Following the work in [35], we randomly sample  $n = 500, 2000$  points per object to get 3D point cloud data. We calculate the pair-wise distance between the point clouds w.r.t. different distance metrics, and then use the K-NN algorithm ( $k = 5$ ) to evaluate the classification accuracy on the testing set. Figure 6(a) summarizes the averaged performance of each metric in 10 trials. Our HCP outperforms other distances on accuracy and requires the least amount of time. See Supplementary Material for more details and results.

**Document classification.** As a typical high-dimensional data classification problem, document classification can be achieved by comparing the Wasserstein distance between two documents' word

<sup>2</sup> $W_2(\mathcal{N}_d(\mathbf{0}_d, \Sigma_X), \mathcal{N}_d(\mathbf{0}_d, \Sigma_Y)) = \text{tr}(\Sigma_X + \Sigma_Y - 2(\Sigma_X^{\frac{1}{2}}\Sigma_Y\Sigma_X^{\frac{1}{2}})^{\frac{1}{2}})^{\frac{1}{2}}$

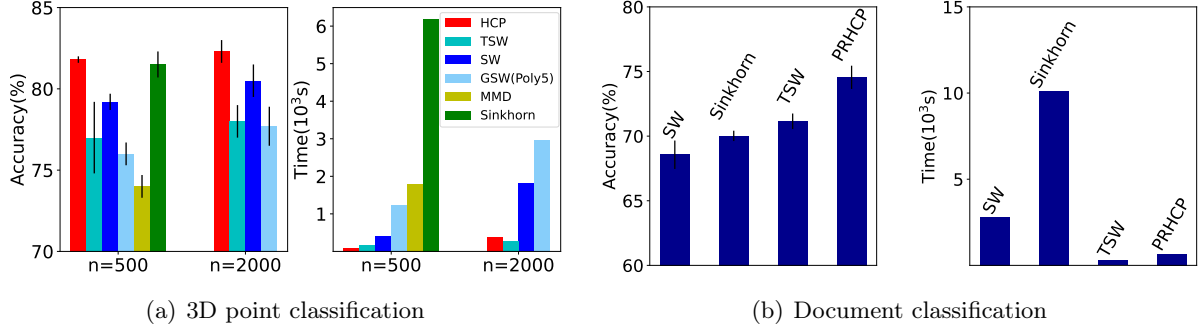


Figure 6: Experimental results in two classification tasks.

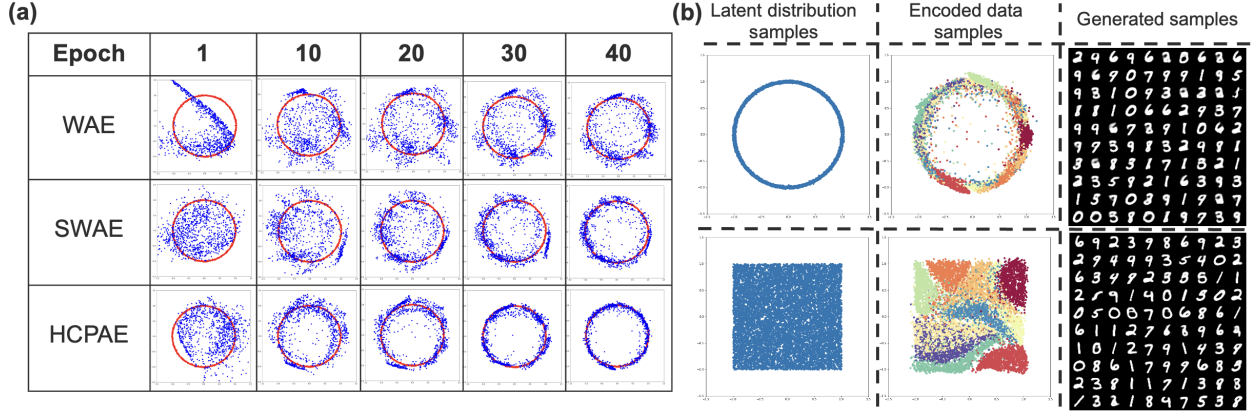


Figure 7: (a) Visualization of these two sample in the latent space during training; (b) Visualization of the encoded samples and the generated images w.r.t. HCP-AE.

embedding sets, as the Word Mover distance [22] does. Our PRHCP distance provides an efficient surrogate of the Wasserstein distance in this problem, which is demonstrated by the following experiment. Following the preprocessing used in [22], we obtain 3,000 documents belonging to three categories from the TWITTER dataset, in which each document is represented as a set of 300-dimensional word embeddings derived by the pre-trained *word2vec* model [28]. We randomly split the dataset into 80% for training and 20% for testing. Similar to the above point cloud classification experiment, we use the K-NN algorithm ( $k = 10$ ) based on different metrics and evaluate the averaged learning results in 10 trials. For PRHCP, we first find the 10-dimensional subspace based on the training data and project testing data to the subspace. Figure 6(b) shows that our PRHCP distance outperforms other distances on classification accuracy, and its runtime is comparable to TSW.

**HCP-based autoencoders.** The proposed distances help us to design new members of Wasserstein autoencoder (WAE) [40]. In particular, when training autoencoders, we leverage HCP, IPRHCP, and PRHCP to penalize the distance between the latent prior distribution and the expected posterior distribution, which leads to three different generative models, denoted as HCP-AE, IPRHCP-AE, and PRHCP-AE. We test these three models in image generation tasks and compare them with the original Wasserstein autoencoder (WAE) [40] and the well-known sliced Wasserstein autoencoder (SWAE) [21]. We first test the capability of HCP-AE in shaping the latent space of the encoder. We train a HCP-AE to encode the MNIST dataset [24] to a two-dimensional latent space (for the sake of visualization), in which both the autoencoding architecture and the hyperparameter setting are

Table 1: Comparisons for various methods on learning image generators

Method	MNIST			CelebA		
	Rec. loss	FID	Epoch Time(s)	Rec. loss	FID	Epoch Time(s)
WAE	11.30	54.61 $\pm$ 0.16	85	68.94	58.12 $\pm$ 0.73	581
SWAE	13.68	42.96 $\pm$ 0.53	70	68.57	84.52 $\pm$ 0.44	536
IPRHCP-AE	11.72	<b>40.03</b> $\pm$ 0.13	83	69.40	<b>56.00</b> $\pm$ 0.08	558
PRHCP-AE	<b>10.07</b>	42.87 $\pm$ 0.46	72	<b>66.65</b>	67.82 $\pm$ 0.21	542



Figure 8: The performance of our generators on face generation and interpolation.

the same as those in [21]. To evaluate the performance, we randomly selected a sample of size 1,000 from the encoded test data points (blue points in Figure 7(a)) and a random sample from the target prior distribution in the latent space (red points in Figure 7(a)). We observed that our HCP-AE convergences much faster than other methods in the latent space. Figure 7(b) visualizes the samples from two different prior distributions in the latent space, the encoded data samples via HCP-AE, and their generated images. The latent codes indeed obey the prior distributions, and the learned models are able to generate high quality images.

Secondly, we test the feasibility of IPRHCP-AE and PRHCP-AE in the cases with high-dimensional latent space. For fairness, all the autoencoders have the same DCGAN-style architecture [36] and hyperparameters and are tested on MNIST and CelebA. The dimension of latent code is 8 for MNIST and 64 for CelebA. We compare the proposed methods with the baselines on *i*) the reconstruction loss on testing samples; *ii*) the Fréchet Inception Distance (FID) [15] between 10,000 testing samples and 10,000 randomly generated samples. Table 1 lists the main differences between IPRHCP-AE, PRHCP-AE and these baselines. Among these autoencoders, our IPRHCP-AE and PRHCP-AE are comparable to the considered alternatives on both testing reconstruction loss and FID score. Some image generation and interpolation results achieved by our methods are shown in Figure 8.

## 6 Conclusion

In this work, we proposed a novel metric for distribution comparison, named Hilbert curve projection (HCP) distance. Thanks to the locality-preserving property of the Hilbert curve projection, the HCP distance enjoys several advantages over the Wasserstein and SW distance. Furthermore, we develop two variants of the HCP distance using (learnable) subspace projections to mitigate the curse-of-dimensionality. In the future, we plan to apply these new metrics to more learning problems and extend them to Gromov-Wasserstein distance and multi-marginal optimal transport.

## References

- [1] Abel, D. J. and D. M. Mark (1990). A comparative analysis of some two-dimensional orderings. *International Journal of Geographical Information Systems* 4(1), 21–31.
- [2] Arjovsky, M., S. Chintala, and L. Bottou (2017). Wasserstein generative adversarial networks. In *International Conference on Machine Learning*, pp. 214–223.
- [3] Bader, M. (2012). *Space-filling curves: an introduction with applications in scientific computing*. Springer.
- [4] Benamou, J.-D., Y. Brenier, and K. Guittet (2002). The Monge–Kantorovitch mass transfer and its computational fluid mechanics formulation. *International Journal for Numerical methods in fluids* 40(1-2), 21–30.
- [5] Bernton, E., P. E. Jacob, M. Gerber, and C. P. Robert (2019). Approximate Bayesian computation with the Wasserstein distance. *Journal of the Royal Statistical Society: Series B (Statistical Methodology)* 81(2), 235–269.
- [6] Bonneel, N., J. Rabin, G. Peyré, and H. Pfister (2015). Sliced and Radon Wasserstein barycenters of measures. *Journal of Mathematical Imaging and Vision* 51(1), 22–45.
- [7] Bonnotte, N. (2013). *Unidimensional and evolution methods for optimal transportation*. Ph. D. thesis, Paris 11.
- [8] Brenier, Y. (1997). A homogenized model for vortex sheets. *Archive for Rational Mechanics and Analysis* 138(4), 319–353.
- [9] Cuturi, M. (2013). Sinkhorn distances: Lightspeed computation of optimal transport. *Advances in Neural Information Processing Systems* 26, 2292–2300.
- [10] Deshpande, I., Y.-T. Hu, R. Sun, A. Pyrros, N. Siddiqui, S. Koyejo, Z. Zhao, D. Forsyth, and A. G. Schwing (2019). Max-sliced Wasserstein distance and its use for GANs. In *Proceedings of the IEEE/CVF Conference on Computer Vision and Pattern Recognition*, pp. 10648–10656.
- [11] Goodfellow, I., J. Pouget-Abadie, M. Mirza, B. Xu, D. Warde-Farley, S. Ozair, A. Courville, and Y. Bengio (2014). Generative adversarial nets. In *Advances in neural information processing systems*, pp. 2672–2680.
- [12] Gretton, A., K. M. Borgwardt, M. J. Rasch, B. Schölkopf, and A. Smola (2012). A kernel two-sample test. *The Journal of Machine Learning Research* 13(1), 723–773.
- [13] Hamilton, C. H. and A. Rau-Chaplin (2008). Compact Hilbert indices: Space-filling curves for domains with unequal side lengths. *Information Processing Letters* 105(5), 155–163.
- [14] He, Z. and A. B. Owen (2016). Extensible grids: uniform sampling on a space filling curve. *Journal of the Royal Statistical Society: Series B (Statistical Methodology)* 78(4), 917–931.
- [15] Heusel, M., H. Ramsauer, T. Unterthiner, B. Nessler, and S. Hochreiter (2017). GANs trained by a two time-scale update rule converge to a local Nash equilibrium. *Advances in neural information processing systems* 30.
- [16] Huang, G., C. Guo, M. J. Kusner, Y. Sun, F. Sha, and K. Q. Weinberger (2016). Supervised word mover’s distance. *Advances in neural information processing systems* 29.

- [17] Imamura, Y., T. Shinohara, K. Hirata, and T. Kuboyama (2016). Fast Hilbert sort algorithm without using Hilbert indices. In *International Conference on Similarity Search and Applications*, pp. 259–267. Springer.
- [18] Kingma, D. P. and J. Ba (2015). Adam: A method for stochastic optimization. *International Conference on Learning Representations*.
- [19] Kingma, D. P. and M. Welling (2014). Auto-encoding variational bayes. *International Conference on Learning Representations*.
- [20] Kolouri, S., K. Nadjahi, U. Simsekli, R. Badeau, and K. Gustavo (2019). Generalized sliced Wasserstein distances. *Advances in Neural Information Processing Systems*.
- [21] Kolouri, S., P. E. Pope, C. E. Martin, and G. K. Rohde (2018). Sliced Wasserstein auto-encoders. In *International Conference on Learning Representations*.
- [22] Kusner, M., Y. Sun, N. Kolkin, and K. Weinberger (2015). From word embeddings to document distances. In *International conference on machine learning*, pp. 957–966. PMLR.
- [23] Le, T., M. Yamada, K. Fukumizu, and M. Cuturi (2019). Tree-sliced variants of Wasserstein distances. In *Advances in Neural Information Processing Systems*.
- [24] LeCun, Y., L. Bottou, Y. Bengio, and P. Haffner (1998). Gradient-based learning applied to document recognition. *Proceedings of the IEEE* 86(11), 2278–2324.
- [25] Lin, T., C. Fan, N. Ho, M. Cuturi, and M. Jordan (2020). Projection robust wasserstein distance and Riemannian optimization. *Advances in neural information processing systems* 33, 9383–9397.
- [26] Lin, T., Z. Zheng, E. Chen, M. Cuturi, and M. I. Jordan (2021). On projection robust optimal transport: Sample complexity and model misspecification. In *International Conference on Artificial Intelligence and Statistics*, pp. 262–270. PMLR.
- [27] Meng, C., Y. Ke, J. Zhang, M. Zhang, W. Zhong, and P. Ma (2019). Large-scale optimal transport map estimation using projection pursuit. *Advances in Neural Information Processing Systems* 32.
- [28] Mikolov, T., I. Sutskever, K. Chen, G. S. Corrado, and J. Dean (2013). Distributed representations of words and phrases and their compositionality. *Advances in neural information processing systems* 26.
- [29] Moon, B., H. V. Jagadish, C. Faloutsos, and J. H. Saltz (2001). Analysis of the clustering properties of the Hilbert space-filling curve. *IEEE Transactions on knowledge and data engineering* 13(1), 124–141.
- [30] Mordant, G. (2021). *Transporting probability measures*. Ph. D. thesis, Université catholique de Louvain.
- [31] Panaretos, V. M. and Y. Zemel (2019). Statistical aspects of Wasserstein distances. *Annual review of statistics and its application* 6, 405–431.
- [32] Paty, F.-P. and M. Cuturi (2019). Subspace robust wasserstein distances. In *International conference on machine learning*, pp. 5072–5081. PMLR.

- [33] Pele, O. and M. Werman (2009). Fast and robust earth mover’s distances. In *2009 IEEE 12th International Conference on Computer Vision*, pp. 460–467. IEEE.
- [34] Peyré, G. and M. Cuturi (2019). Computational optimal transport: With applications to data science. *Foundations and Trends® in Machine Learning* 11(5-6), 355–607.
- [35] Qi, C. R., H. Su, K. Mo, and L. J. Guibas (2017). Pointnet: Deep learning on point sets for 3d classification and segmentation. In *Proceedings of the IEEE conference on computer vision and pattern recognition*, pp. 652–660.
- [36] Radford, A., L. Metz, and S. Chintala (2016). Unsupervised representation learning with deep convolutional generative adversarial networks. *International Conference on Learning Representations*.
- [37] Rakotomamonjy, A., A. Traoré, M. Berar, R. Flamary, and N. Courty (2018). Distance measure machines. *arXiv preprint arXiv:1803.00250*.
- [38] Rubner, Y., L. J. Guibas, and C. Tomasi (1997). The earth mover’s distance, multi-dimensional scaling, and color-based image retrieval. In *Proceedings of the ARPA image understanding workshop*, Volume 661, pp. 668.
- [39] Tanaka, A. (2001). *Study on a fast ordering of high dimensional data to spatial index*. Ph. D. thesis, Master thesis, Kyushu Institute of Technology.
- [40] Tolstikhin, I., O. Bousquet, S. Gelly, and B. Schölkopf (2018). Wasserstein auto-encoders. In *6th International Conference on Learning Representations*.
- [41] Villani, C. (2009). *Optimal transport: old and new*, Volume 338. Springer.
- [42] Wu, Z., S. Song, A. Khosla, F. Yu, L. Zhang, X. Tang, and J. Xiao (2015). 3d shapenets: A deep representation for volumetric shapes. In *Proceedings of the IEEE conference on computer vision and pattern recognition*, pp. 1912–1920.
- [43] Zhang, J., P. Ma, W. Zhong, and C. Meng. Projection-based techniques for high-dimensional optimal transport problems. *Wiley Interdisciplinary Reviews: Computational Statistics*, e1587.
- [44] Zumbusch, G. (2012). *Parallel multilevel methods: adaptive mesh refinement and loadbalancing*. Springer Science & Business Media.

# Supplementary Material for "Hilbert Curve Projection Distance for Distribution Comparison"

Section A includes the proof of all theorems, propositions, corollaries and remarks. We prove the HCP distance is a well-defined metric and it converges to its population counterpart at a rate of no more than  $O(n^{-1/2d})$ . We also prove some inequalities about IPRHCP. Section B includes implementation details and more experimental results for Section 5. Section C gives some additional analysis. We first provide an intuition on why SW distance and its invariants tend to converge slower than HCP distance. We then verify the robustness of PRHCP distance, illustrate the empirical sample complexity of the proposed distances, and study the effect of order  $k$  in HCP distance.

## A Technical details for the proof

The Hilbert curve enjoys three properties, see [44; 14] for details.

1. Let  $\lambda_d$  be the  $d$ -dimensional Lebesgue measure. For any measurable set  $\Omega \subseteq [0, 1]^d$ , one has  $\lambda_1(\Omega) = \lambda_d(H(\Omega))$ .
2. If a random variable  $X$  follows the uniform distribution on  $[0, 1]^d$ , then  $H(X)$  follows the uniform distribution on  $[0, 1]$ . This is to say, one has  $\int_{[0, 1]^d} f(\mathbf{x}) d\mathbf{x} = \int_0^1 f[H(x)] dx$ .
3. For any  $x, y \in [0, 1]$ , one has  $\|H(x) - H(y)\| \leq 2\sqrt{d+3}|x - y|^{1/d}$ .

We first provide two essential lemmas.

**Lemma 1.** *If a random variable  $Z$  follows the probability distribution function  $g_\mu$ , then  $H_\mu(Z)$  follows the probability density function  $f_\mu$ .*

*Proof.* Without losing generality, we assume  $\tilde{\Omega}_\mu = [0, 1]^d$ . We only need to prove that  $Pr(H_\mu(Z) \in A) = \int_A f_\mu$  for any measurable set  $A$ . By property 2 of Hilbert curve, we have  $\int_{[0, 1]^d} f_\mu(\mathbf{x}) \mathbf{1}_A d\mathbf{x} = \int_0^1 f_\mu[H_\mu(x)] \mathbf{1}_A[H_\mu(x)] dx$ . As a result, one has

$$\begin{aligned} \int_A f_\mu &= \int_{[0, 1]^d} f_\mu(\mathbf{x}) \mathbf{1}_A d\mathbf{x} \\ &= \int_0^1 f_\mu[H_\mu(x)] \mathbf{1}_A[H_\mu(x)] dx \\ &= \int_{\{x: x \in H_\mu(A)\}} f_\mu[H_\mu(x)] dx \\ &= Pr(H_\mu(Z) \in A) \end{aligned}$$

□

**Lemma 2.** *Let  $\{X_i\}_{i=1}^n$  and  $\{Y_i\}_{i=1}^n$  be two i.i.d. samples, which are generated from probability measures  $\mu$  and  $\nu$ , respectively. Let  $\{X_{(i)}^*\}_{i=1}^n$  and  $\{Y_{(i)}^*\}_{i=1}^n$  be the sorted samples along the Hilbert curves  $H_\mu$  and  $H_\nu$ , respectively. Then,  $\mathbb{E} \sum_{i=1}^n \|X_{(i)}^* - Y_{(i)}^*\|_p^p / n \rightarrow HCP_p^p(\mu, \nu)$ , as  $n \rightarrow \infty$ .*

*Proof.* Let  $\{X_i^g\}_{i=1}^n$  and  $\{Y_i^g\}_{i=1}^n$  be two i.i.d. samples, which are generated from  $g_\mu$  and  $g_\nu$ , respectively. Let  $\hat{g}_\mu(t) = \sum \mathbf{1}_{\{t \geq X_i^g\}} / n$ ,  $\hat{g}_\nu(t) = \sum \mathbf{1}_{\{t \geq Y_i^g\}} / n$ , where  $X_{(r)}^g, Y_{(r)}^g$  are the  $r$ -th order statistics.

$$\begin{aligned} \widehat{HCP}_p^p(\mu, \nu) &= \int_0^1 \|H_\mu(\hat{g}_\mu^{-1}(t)) - H_\nu(\hat{g}_\nu^{-1}(t))\|_p^p dt \\ &= \sum_{i=1}^n \|H_\mu(X_{(i)}^g) - H_\nu(Y_{(i)}^g)\|_p^p / n \end{aligned}$$

By Lemma 1, we know that

$$\mathbb{E} \frac{1}{n} \sum \|H_\mu(X_{(i)}^g) - H_\nu(Y_{(i)}^g)\|_p^p = \mathbb{E} \frac{1}{n} \sum_{i=1}^n \|X_{(i)}^* - Y_{(i)}^*\|_p^p$$

Hence, we only need to prove that

$$\mathbb{E} \int_0^1 \|H_\mu(\hat{g}_\mu^{-1}(t)) - H_\nu(\hat{g}_\nu^{-1}(t))\|_p^p dt \rightarrow \int_0^1 \|H_\mu(g_\mu^{-1}(t)) - H_\nu(g_\nu^{-1}(t))\|_p^p dt$$

as  $n \rightarrow \infty$ .

Clearly, considered that  $H_\mu, H_\nu$  are all bounded, we know that for any fixed  $t \in [0, 1]$ ,

$$\mathbb{E} \|H_\mu(\hat{g}_\mu^{-1}(t)) - H_\nu(\hat{g}_\nu^{-1}(t))\|_p^p \rightarrow \|H_\mu(g_\mu^{-1}(t)) - H_\nu(g_\nu^{-1}(t))\|_p^p$$

Thus, by dominated convergence theorem, we have

$$\int_0^1 \mathbb{E} \|H_\mu(\hat{g}_\mu^{-1}(t)) - H_\nu(\hat{g}_\nu^{-1}(t))\|_p^p dt \rightarrow \int_0^1 \|H_\mu(g_\mu^{-1}(t)) - H_\nu(g_\nu^{-1}(t))\|_p^p dt$$

as  $n \rightarrow \infty$ . Finally, because  $H_\mu, H_\nu$  are all bounded, we have proved it.  $\square$

**Theorem 3.**  $HCP_p(\mu, \nu)$  is a well-defined metric over all absolutely continuous probability measures in  $\mathcal{P}_p(\Omega)$  and  $W_p(\mu, \nu) \leq HCP_p(\mu, \nu)$ .

*Proof.* Lemma 2 tells us that  $\mathbb{E} \frac{1}{n} \sum_{i=1}^n \|X_{(i)}^* - Y_{(i)}^*\|_p^p \rightarrow HCP_p^p(\mu, \nu)$ , as  $n \rightarrow \infty$ . And we know that  $\mathbb{E} \inf_\sigma \frac{1}{n} \sum_{i=1}^n \|X_i - Y_{\sigma(i)}\|_p^p \rightarrow W_p^p(\mu, \nu)$ , as  $n \rightarrow \infty$ . Clearly,  $\inf_\sigma \frac{1}{n} \sum_{i=1}^n \|X_i - Y_{\sigma(i)}\|_p^p \leq \frac{1}{n} \sum_{i=1}^n \|X_{(i)}^* - Y_{(i)}^*\|_p^p$ . Hence, we have  $W_p(\mu, \nu) \leq HCP_p(\mu, \nu)$ .

By definition of HCP, it's clear that  $HCP_p(\mu, \nu) \geq 0$  and  $HCP_p(\mu, \nu) = HCP_p(\nu, \mu)$ . Because Wasserstein distance is a well-define metric, we can easily get  $HCP_p(\mu, \nu) = 0$  if and only if  $\mu = \nu$ . Next, we prove the triangle inequality.

$$\begin{aligned} HCP_p(\mu, \nu) &= \left( \int_0^1 \|H_\mu(g_\mu^{-1}(t)) - H_\nu(g_\nu^{-1}(t))\|_p^p dt \right)^{1/p} \\ &= \left( \int_0^1 \theta_{\mu, \nu}(t)^p dt \right)^{1/p} \\ &\leq \left( \int_0^1 \theta_{\mu, \tau}(t)^p dt \right)^{1/p} + \left( \int_0^1 |\theta_{\mu, \nu}(t) - \theta_{\mu, \tau}(t)|^p dt \right)^{1/p} \\ &\leq \left( \int_0^1 \theta_{\mu, \tau}(t)^p dt \right)^{1/p} + \left( \int_0^1 \theta_{\nu, \tau}(t)^p dt \right)^{1/p} \\ &= HCP_p(\mu, \tau) + HCP_p(\nu, \tau) \end{aligned}$$

where first inequality uses Minkowski inequality and the second uses triangle inequality.  $\square$

To prove the next Theorem, we first provide two essential lemmas.

**Lemma 3.** Let  $\tilde{\Omega}_\mu = \prod_i [a^{(i)}, b^{(i)}]$  and  $\mathbf{X} \sim \mu$  be random vector. Denote  $\tilde{\Omega}_{\mu_n}^i$  be the  $i$ -th side of rectangle  $\tilde{\Omega}_{\mu_n}$  and  $\mathbf{X}^{(i)}$  be  $i$ -th variable of  $\mathbf{X}$ . If  $Pr(\mathbf{X}^{(i)} - a^{(i)} < n^{-1/2}) \leq n^{-1/2}$ ,  $Pr(b^{(i)} - \mathbf{X}^{(i)} > n^{-1/2}) \leq n^{-1/2}$  for all  $i = 1, \dots, d$ , we have  $Pr(A^c) \lesssim n^{-1/2}$  where  $A = \{|\tilde{\Omega}_{\mu_n}^i - \tilde{\Omega}_\mu^i| \leq n^{-1/2}, \forall i\}$ .



*Proof.* Without loss of generality, we assume  $\tilde{\Omega}_\mu = [0, 1]^d$ . For the  $i$ -th dimension, directly calculation yields that

$$Pr(\min_j \mathbf{X}_j^{(i)} > n^{-1/2}) = 1 - (1 - Pr(\mathbf{X}_j^{(i)} \leq n^{-1/2}))^n = 1 - (1 - \frac{1}{n^{1/2}})^n \rightarrow 1 - e^{-n^{-1/2}}.$$

Similarly

$$Pr(1 - \max_j \mathbf{X}_j^{(i)} > n^{-1/2}) = 1 - (Pr(\mathbf{X}_j^{(i)} \leq 1 - n^{-1/2}))^n = 1 - (1 - \frac{1}{n^{1/2}})^n \rightarrow 1 - e^{-n^{-1/2}}.$$

Note that  $1 - e^{-n^{-1/2}} = O(n^{-1/2})$ . The result follows.  $\square$

**Lemma 4.** Assume that for every sample point  $\mathbf{x}_i$  corresponds to  $H_{\mu_n}(s_i)$  where  $i = 1, 2, \dots, n$ , it holds that  $\int_{s_i - cn^{-1/2}}^{s_i + cn^{-1/2}} f_\mu(H_\mu(s))ds \geq cn^{-1/2}$  for  $c \in [0, \infty)$ . Then, we have  $|g_\mu^{-1}(t) - g_{\mu_n}^{-1}(t)| \lesssim n^{-1/2}$  in probability.

*Proof.* Now we first show that for any  $t_0 \in [0, 1]$ , it holds that

$$\left| \int_0^{t_0} f_\mu(H_\mu(s))ds - \int_0^{t_0} f_{\mu_n}(H_{\mu_n}(s))ds \right| \lesssim n^{-1/2}. \quad (6)$$

Simple calculation yields that

$$\left| \int_0^{t_0} f_\mu(H_\mu(s))ds - \int_0^{t_0} f_{\mu_n}(H_{\mu_n}(s))ds \right| \quad (7)$$

$$\leq \left| \int_0^{t_0} f_\mu(H_\mu(s))ds - \int_0^{t_0} f_{\mu_n}(H_\mu(s))ds \right| + \left| \int_0^{t_0} f_{\mu_n}(H_\mu(s))ds - \int_0^{t_0} f_{\mu_n}(H_{\mu_n}(s))ds \right|. \quad (8)$$

For the first term, denote  $E$  be the area that covered by  $\{H_\mu(s) : s \in [0, t_0]\}$ . Thus by the second properties of the Hilbert curve, we have

$$\int_E f_\mu(\mathbf{x})d\mathbf{x} = \int_0^{t_0} f_\mu(H_\mu(s))ds.$$

For the empirical measure, according to the central limit theory, one can see that

$$\left| \int_E f_{\mu_n}(\mathbf{x})d\mathbf{x} - \int_E f_\mu(\mathbf{x})d\mathbf{x} \right| = O_P(n^{-1/2}).$$

Thus the first term satisfies that

$$\left| \int_0^{t_0} f_\mu(H_\mu(s))ds - \int_0^{t_0} f_{\mu_n}(H_{\mu_n}(s))ds \right| \lesssim n^{-1/2}.$$

Without loss of generality, we assume  $\tilde{\Omega}_\mu = [0, 1]^d$ . Directly calculation yields that the difference between area covered by  $\{H_\mu(s) : s \in [0, 1]\}$  and  $\{H_{\mu_n}(s) : s \in [0, 1]\}$  can be bounded by

$$1 - (1 - \frac{2}{n^{1/2}})^d = 1 - 1 + \frac{2d}{n^{1/2}} + o(n^{-1/2}),$$

if  $A$  defined in Lemma 3 happens. Clearly, there are  $O(n^{-1/2})$  proportion of sample points that will be in  $\{H_\mu(s) : s \in [0, t_0]\}$  but not  $\{H_{\mu_n}(s) : s \in [0, t_0]\}$  with probability approaching one. That is to say, the second term is bounded by  $O_P(n^{-1/2})$ .

We can conclude that

$$\left| \int_0^{t_0} f_\mu(H_\mu(s))ds - \int_0^{t_0} f_{\mu_n}(H_{\mu_n}(s))ds \right| \lesssim n^{-1/2}. \quad (9)$$

Let  $x_0 = g_{\mu_n}^{-1}(t)$ . It is straightforward to see that  $|\int_0^{x_0} f_\mu(H_\mu(s))ds - t| \lesssim n^{-1/2}$ . By the definition of  $g_{\mu_n}^{-1}(t)$ , we know  $H_{\mu_n}(x_0)$  corresponds to a sample point. Under the assumption that every sample point  $\mathbf{x}_i$  corresponds to  $H_{\mu_n}(s_i)$ , it holds that  $\int_{s_i - cn^{-1/2}}^{s_i + cn^{-1/2}} f_\mu(H_\mu(s))ds \gtrsim cn^{-1/2}$ . The results follow.  $\square$

Next, we prove a theorem of the convergence rate about HCP.

**Theorem 4.** *Let  $\mu$  be an absolutely continuous probability measure, whose probability density has bounded non-zero support  $\Omega$  in  $d$ -dimensional space, and  $\mu_n$  is the empirical distribution based on  $n$  samples. Let  $\tilde{\Omega}_\mu = \prod_{i=1}^d [a^{(i)}, b^{(i)}]$  be the smallest hyper-rectangle covering  $\Omega$ . If below two conditions are satisfied,*

**Condition 1:**

*$Pr(\mathbf{X}^{(i)} - a^{(i)} < n^{-1/2}) \leq n^{-1/2}$  and  $Pr(b^{(i)} - \mathbf{X}^{(i)} > n^{-1/2}) \leq n^{-1/2}$  hold for all  $i = 1, \dots, d$  where  $\mathbf{X} \sim \mu$  be random vector,  $\mathbf{X}^{(i)}$  be  $i$ -th variable of  $\mathbf{X}$ .*

**Condition 2:** *For every sample point  $\mathbf{x}_j$  corresponds to  $H_{\mu_n}(s_j)$  where  $j = 1, 2, \dots, n$ , it holds that  $\int_{s_j - cn^{-1/2}}^{s_j + cn^{-1/2}} f_\mu(H_\mu(s))ds \geq cn^{-1/2}$  for  $c \in [0, \infty)$ .*

*then  $\mathbb{E}[HCP_p(\mu, \mu_n)] \gtrsim n^{-\frac{1}{d}}$  and  $\mathbb{E}[HCP_p(\mu, \mu_n)] \lesssim n^{-\frac{1}{2d}}$ .*

*Proof.* The lower bound is easy to prove. From statistical conclusions of empirical Wasserstein distance [31], we know that

$$\mathbb{E}[W_p(\mu, \mu_n)] \gtrsim n^{-\frac{1}{d}}$$

Because  $W_p(\mu, \mu_n) \leq HCP_p(\mu, \mu_n)$ , we have

$$\mathbb{E}[HCP_p(\mu, \mu_n)] \gtrsim n^{-\frac{1}{d}}$$

The upper bound is not very trivial. Considering that  $H_\mu$  is a linear stretching of  $H$  and using Cauchy-Schwarz inequality, we have  $\|H_\mu(x) - H_\mu(y)\|_2 \leq C_\mu \|H(x) - H(y)\|_2 \leq 2C_\mu \sqrt{d+3} |x-y|^{1/d}$  for any  $x, y \in [0, 1]$ . And by equivalence of vector norms, we have  $\|H_\mu(x) - H_\mu(y)\|_p \leq C_p \|H_\mu(x) - H_\mu(y)\|_2 \leq 2C_\mu C_p \sqrt{d+3} |x-y|^{1/d}$ , where  $C_p, C_\mu$  are two constants.

By definition,

$$\begin{aligned} HCP_p(\mu, \mu_n) &= \left( \int_0^1 \|H_\mu(g_\mu^{-1}(t)) - H_{\mu_n}(g_{\mu_n}^{-1}(t))\|_p^p dt \right)^{1/p} \\ &\leq \left( \int_0^1 \|H_\mu(g_\mu^{-1}(t)) - H_{\mu_n}(g_\mu^{-1}(t))\|_p^p dt \right)^{1/p} + \\ &\quad \left( \int_0^1 \|H_{\mu_n}(g_\mu^{-1}(t)) - H_{\mu_n}(g_{\mu_n}^{-1}(t))\|_p^p dt \right)^{1/p} \end{aligned}$$

For the first part, because of Condition 1 and Lemma 3, we have

$$\left( \int_0^1 \|H_\mu(g_\mu^{-1}(t)) - H_{\mu_n}(g_\mu^{-1}(t))\|_p^p dt \right)^{1/p} \leq d^{1/p} n^{-1/d} Pr(A) + M Pr(A^c) \lesssim n^{-1/d}$$

For the second part, because of Condition 2 and Lemma 4, we have

$$\begin{aligned} \left( \int_0^1 \|H_{\mu_n}(g_\mu^{-1}(t)) - H_{\mu_n}(g_{\mu_n}^{-1}(t))\|_p^p dt \right)^{1/p} &\lesssim \left( \int_0^1 |g_\mu^{-1}(t) - g_{\mu_n}^{-1}(t)|^{p/d} dt \right)^{1/p} \\ &\lesssim \left( \int_0^1 n^{-p/(2d)} dt \right)^{1/p} \\ &= n^{-1/2d} \end{aligned}$$

□

**Corollary 2.** *The lower bound shown in Theorem 4 is achievable: If  $\mu$  is uniformly distributed on  $[0, 1]^d$  and the  $n$  sample points lie uniformly on the Hilbert curve, then  $\mathbb{E}[HCP_p(\mu, \mu_n)] = O(n^{-\frac{1}{d}})$ .*

*Proof.* Note that in this case  $H_{\mu_n}(0)$  corresponds to  $(0, \dots, 0)^T$  and  $H_{\mu_n}(1)$  corresponds to  $(1, \dots, 1)^T$ . Thus  $\tilde{\Omega}_\mu = \tilde{\Omega}_{\mu_n}$ .

By definition,

$$\begin{aligned} HCP_p(\mu, \mu_n) &= \left( \int_0^1 \|H_\mu(g_\mu^{-1}(t)) - H_{\mu_n}(g_{\mu_n}^{-1}(t))\|_p^p dt \right)^{1/p} \\ &\leq \left( \int_0^1 \|H_\mu(g_\mu^{-1}(t)) - H_{\mu_n}(g_\mu^{-1}(t))\|_p^p dt \right)^{1/p} + \\ &\quad \left( \int_0^1 \|H_{\mu_n}(g_\mu^{-1}(t)) - H_{\mu_n}(g_{\mu_n}^{-1}(t))\|_p^p dt \right)^{1/p} \end{aligned}$$

For the first part, we have

$$\left( \int_0^1 \|H_\mu(g_\mu^{-1}(t)) - H_{\mu_n}(g_\mu^{-1}(t))\|_p^p dt \right)^{1/p} \leq d^{1/p} n^{-1/d} \lesssim n^{-1/d}$$

Now we consider the second term,

$$\left( \int_0^1 \|H_{\mu_n}(g_\mu^{-1}(t)) - H_{\mu_n}(g_{\mu_n}^{-1}(t))\|_p^p dt \right)^{1/p} \lesssim \left( \int_0^1 |g_\mu^{-1}(t) - g_{\mu_n}^{-1}(t)|^{p/d} dt \right)^{1/p}.$$

Thus it is sufficient to show that  $|g_\mu^{-1}(t) - g_{\mu_n}^{-1}(t)|$  is  $O(n^{-1})$ . Let  $E_i = H(I_i)$  with  $I_i$  being the interval  $[\frac{i-1}{n}, \frac{i}{n})$ . It follows  $\int_{E_i} 1 d\mathbf{x} = n^{-1}$ . Thus for any  $t \in [\frac{i-1}{n}, \frac{i}{n})$  we have  $i/n = g_{\mu_n}^{-1}(t)$ . Also note that  $\int_0^{(i-1)/n} f_\mu(H_\mu(s)) ds = (i-1)/n$  and  $\int_0^{i/n} f_\mu(H_\mu(s)) ds = i/n$ . Since  $f_\mu > 0$  in  $\Omega_\mu$  thus  $g_\mu^{-1}(t)$  must lie in  $[\frac{i-1}{n}, \frac{i}{n})$  when  $t \in [\frac{i-1}{n}, \frac{i}{n})$ , which implies  $|g_\mu^{-1}(t) - g_{\mu_n}^{-1}(t)|$  is  $O(n^{-1})$ . The desired result holds by simple calculations.

□

**Remark 4.** *One byproduct of Theorem 4 is that it indicates when  $k = O(\log(n))$ , replacing the Hilbert curve with the  $k$ -order Hilbert curve  $\hat{H}_k$  in the HCP distance will not affect its convergence rate.*

*Proof.* Theorem 4 indicates that  $|\int_0^{t_0} f_\mu(H_\mu(s)) ds - \int_0^{t_0} f_{\mu_n}(H_\mu(s)) ds| \lesssim n^{-1/2}$ , and one has  $\{\hat{H}_k(t) : t \in [0, (s+1)/2^{dk}]\} \supset \{H(t) : t \in [0, t_0]\} \supset \{\hat{H}_k(t) : t \in [0, s/2^{dk}]\}$  for every  $t_0 \in I_d^k(s) = [s/2^{dk}, (s+1)/2^{dk}]$  because  $H(I_d^k(s)) = \hat{H}_k(I_d^k(s))$ . Therefore, when approximating  $H$  by  $\hat{H}_k$ , the approximation error can be ignored when  $n^{-1/2} = o(2^{-dk})$ , which implies  $k$  is at least be the same order compared with  $\log(n)$ .

□

**Remark 5.** If we replace  $\mathbb{S}_{d,q}$  in Definition of IPRHCP with matrix set  $\{\mathbf{E} \in \mathbb{R}^{d \times q} : \mathbf{E}^\top \mathbf{E} = \mathbf{J}_q\}$  where  $\mathbf{J}_k$  is a  $k \times k$  all ones matrix, we have  $\text{IPRHCP}_{p,q}(\mu, \nu) = q^{1/p} \text{SW}_p(\mu, \nu)$ .

*Proof.* Here, we take  $q = 2$  as an example. It can be easily extended to the case  $q > 2$ . From the construction of 2-d Hilbert Curve, we know that if  $x_1 < x_2$  and  $H^{-1}((x_1, x_1)), H^{-1}((x_2, x_2))$  exist (don't exist only on a measure 0 set), then  $H^{-1}((x_1, x_1)) < H^{-1}((x_2, x_2))$ . By  $\mathbf{E}^\top \mathbf{E} = \mathbf{J}_2$ , we know  $\mathbf{E} = (\mathbf{v}, \mathbf{v})$  with  $\|\mathbf{v}\|_2 = 1$ . Hence, we can easily conclude that

$$\text{HCP}_p^p(P_{\mathbf{E}\#}\mu, P_{\mathbf{E}\#}\nu) = 2W_p^p(P_{\mathbf{v}\#}\mu, P_{\mathbf{v}\#}\nu)$$

Thus,

$$\begin{aligned} \text{IPRHCP}_{p,q}(\mu, \nu) &= \left( \int \text{HCP}_p^p(P_{\mathbf{E}\#}\mu, P_{\mathbf{E}\#}\nu) d\sigma(\mathbf{E}) \right)^{1/p} \\ &= \left( \int_{\mathbb{S}_{d,1}} 2W_p^p(P_{\mathbf{v}\#}\mu, P_{\mathbf{v}\#}\nu) d\sigma(\mathbf{v}) \right)^{1/p} \\ &= 2^{1/p} \text{SW}_p(\mu, \nu) \end{aligned}$$

□

**Proposition 3.**  $\text{IPRHCP}_{p,q}(\mu, \nu)$  is a well-defined metric over all absolutely continuous probability measures in  $\mathcal{P}_p(\Omega)$  and  $\text{IPRW}_{p,q}(\mu, \nu) \leq \text{IPRHCP}_{p,q}(\mu, \nu)$ .

*Proof.* By definition of IPRHCP and Theorem 3

$$\begin{aligned} \text{IPRHCP}_{p,q}(\mu, \nu) &= \left( \int_{\mathbb{S}_{d,q}} \text{HCP}_p^p(P_{\mathbf{E}\#}\mu, P_{\mathbf{E}\#}\nu) d\sigma(\mathbf{E}) \right)^{1/p} \\ &\geq \left( \int_{\mathbb{S}_{d,q}} W_p^p(P_{\mathbf{E}\#}\mu, P_{\mathbf{E}\#}\nu) d\sigma(\mathbf{E}) \right)^{1/p} \\ &= \text{IPRW}_{p,q}(\mu, \nu) \end{aligned}$$

By definition of IPRHCP, it's clear that  $\text{IPRHCP}_{p,q}(\mu, \nu) \geq 0$  and  $\text{IPRHCP}_{p,q}(\mu, \nu) = \text{IPRHCP}_{p,q}(\nu, \mu)$ . Because  $\text{IPRW}_{p,q}$  is a well-defined metric, we can easily get  $\text{IPRHCP}_{p,q}(\mu, \nu) = 0$  if and only if  $\mu = \nu$ . Next, we prove the triangle inequality. Indeed, this can be directly deduced by Minkowski inequality. To be more precise,

$$\begin{aligned} \text{IPRHCP}_{p,q}(\mu, \nu) &= \left( \int_{\mathbb{S}_{d,q}} \text{HCP}_p^p(P_{\mathbf{E}\#}\mu, P_{\mathbf{E}\#}\nu) d\sigma(\mathbf{E}) \right)^{1/p} \\ &\leq \left( \int_{\mathbb{S}_{d,q}} [\text{HCP}_p(P_{\mathbf{E}\#}\mu, P_{\mathbf{E}\#}\tau) + \text{HCP}_p(P_{\mathbf{E}\#}\nu, P_{\mathbf{E}\#}\tau)]^p d\sigma(\mathbf{E}) \right)^{1/p} \\ &\leq \text{IPRHCP}_{p,q}(\mu, \tau) + \text{IPRHCP}_{p,q}(\nu, \tau) \end{aligned}$$

where first inequality uses triangle inequality from Theorem 3 and the second uses Minkowski inequality. □

**Proposition 4.**  $\text{SW}_p^p(\mu, \nu) \leq \alpha_{q,p} \text{IPRHCP}_{p,q}^p(\mu, \nu)$ , where  $\alpha_{q,p} = \int_{\mathbb{S}_{q,1}} \|\theta\|_p^p d\theta / q \leq 1$ . As a special case, when  $p = 2$ , one has  $\alpha_{q,2} = 1/q$  and  $\text{SW}_2(\mu, \nu) \leq \text{IPRHCP}_{2,q}(\mu, \nu) / \sqrt{q}$ .

*Proof.* First, we introduce an inequality between W and SW distance, which has been proved in [7]. When  $c(x, y) = \|x - y\|^p$  for  $p \geq 2$ , the following upper bound hold for the SW distance :

$$\text{SW}_p^p(\mu, \nu) \leq \alpha_{d,p} W_p^p(\mu, \nu)$$

where,  $\alpha_{d,p} = \frac{1}{d} \int_{\mathbb{S}_{d,1}} \|\theta\|_p^p d\theta \leq 1$ .

Thus, we have:

$$\begin{aligned} \text{IPRHCP}_{p,q}^p(\mu, \nu) &= \int_{\mathbb{S}_{d,q}} \text{HCP}_p^p(P_{\mathbf{E}\#}\mu, P_{\mathbf{E}\#}\nu) d\sigma(\mathbf{E}) \\ &\geq \int_{\mathbb{S}_{d,q}} W_p^p(P_{\mathbf{E}\#}\mu, P_{\mathbf{E}\#}\nu) d\sigma(\mathbf{E}) \\ &\geq \int_{\mathbb{S}_{d,q}} \frac{1}{\alpha_{q,p}} \text{SW}_p^p(P_{\mathbf{E}\#}\mu, P_{\mathbf{E}\#}\nu) d\sigma(\mathbf{E}) \\ &= \frac{1}{\alpha_{q,p}} \int_{\mathbb{S}_{d,q}} \int_{\mathbb{S}_{q,1}} W_p^p(P_{\mathbf{v}\#}[P_{\mathbf{E}\#}\mu], P_{\mathbf{v}\#}[P_{\mathbf{E}\#}\nu]) d\sigma(\mathbf{v}) d\sigma(\mathbf{E}) \\ &= \frac{1}{\alpha_{q,p}} \int_{\mathbb{S}_{d,1}} W_p^p(P_{\mathbf{v}\#}\mu, P_{\mathbf{v}\#}\nu) d\sigma(\mathbf{v}) \\ &= \frac{1}{\alpha_{q,p}} \text{SW}_p^p(\mu, \nu), \end{aligned}$$

where first inequality uses Theorem 3, second inequality uses the above inequality and the last several equalities use the property of SW. □

## B Implementation details and more experimental results for Section 5

### B.1 Approximation of Wasserstein flow

We considered a circle-shape distribution for the target in the experiment of Wasserstein flow. Other settings remain the same, and the results are shown in Fig. 9.

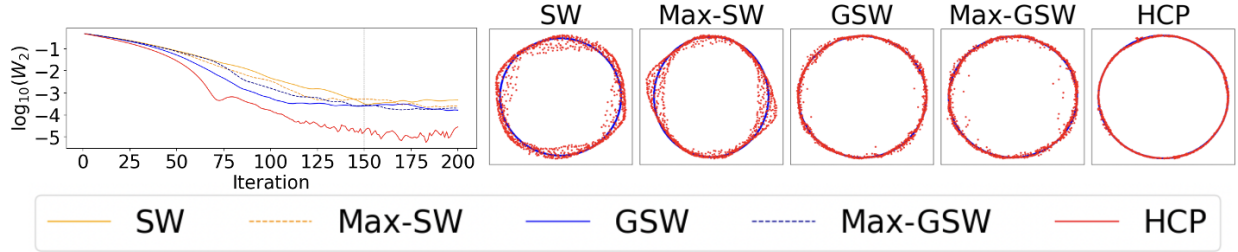


Figure 9: Left: Log 2-Wasserstein distance between the source and target distributions versus the number of iterations  $t$ . Right: A snapshot when  $t = 150$ .

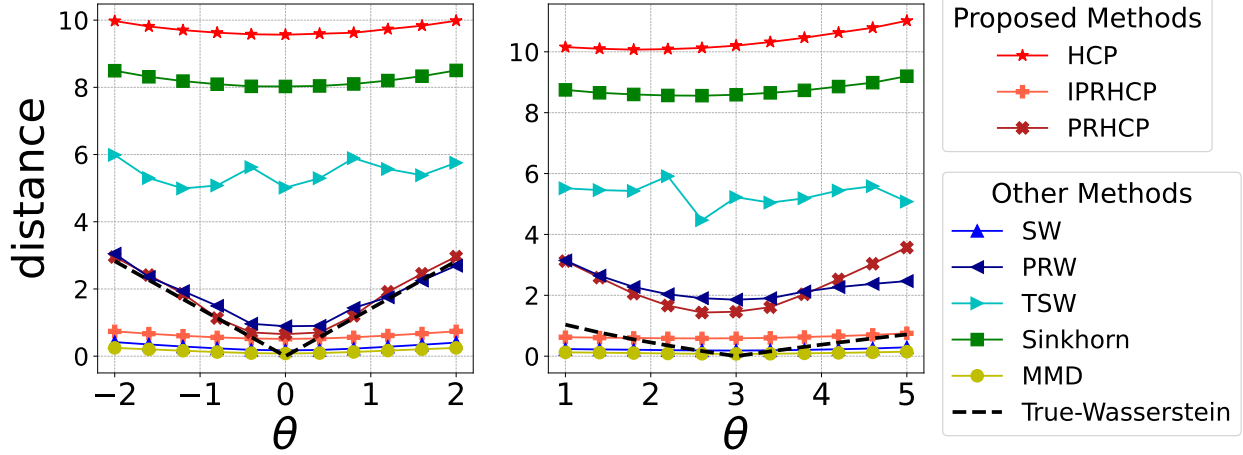


Figure 10: Distances versus different  $\theta$ .

## B.2 Effectiveness and efficiency for high-dimensional data

We provide synthetic data analysis to show which metric provides a reasonable distance between two high-dimensional Gaussian distributed samples. Let  $\{\mathbf{x}_i\}_{i=1}^n$  and  $\{\mathbf{y}_i\}_{i=1}^n$  be two i.i.d. samples generated from  $\mathcal{N}_d(\boldsymbol{\mu}_X, \boldsymbol{\Sigma}_X)$  and  $\mathcal{N}_d(\boldsymbol{\mu}_Y, \boldsymbol{\Sigma}_Y)$ , respectively. We considered two different settings as follows.

1.  $\boldsymbol{\mu}_X = \mathbf{0}_d$ ,  $\boldsymbol{\mu}_Y = (\theta, \theta, 0, \dots, 0)^\top$ ,  $\boldsymbol{\Sigma}_X = \boldsymbol{\Sigma}_Y = \mathbf{I}_d$ .
2.  $\boldsymbol{\mu}_X = \boldsymbol{\mu}_Y = \mathbf{0}_d$ ,  $\boldsymbol{\Sigma}_X = \begin{pmatrix} 3 & 0 & 0 \\ 0 & 3 & 0 \\ 0 & 0 & \mathbf{I}_{d-2} \end{pmatrix}$ ,  $\boldsymbol{\Sigma}_Y = \begin{pmatrix} \theta & 0 & 0 \\ 0 & \theta & 0 \\ 0 & 0 & \mathbf{I}_{d-2} \end{pmatrix}$ .

Let  $n = 200$  and  $d = 50$ . We repeated each experiment a hundred times and took the average. The results are shown in Fig. 10, where each method is labeled by a colored line. We also calculated the true Wasserstein distance using its closed-form expression between two Gaussian distributions. For these two settings, PRW and PRHCP are the only two that perform similarly as the true Wasserstein distance.

## B.3 3D point cloud classification

We used the RBF kernel for MMD, and we set the number of slices  $n_s = 10$  for SW,  $n_s = 10, T = 7, \kappa = 4$  for TSW. Here,  $T$  is the predefined deepest level of the tree,  $n_s$  is the number of slices and  $\kappa$  is the number of clusters. The raw CAD models dataset contains the information for edges and vertices, as shown in Fig. 11(a). Following the pipeline in [35], we uniformly sampled  $n$  data points on mesh faces according to face area and normalized them. The processed data is visualized in Fig. 11(b) and numerical results are summarized in Table 2. We observed that the proposed HCP distance leads to the best or the second best accuracy, requiring the shortest CPU time in most of the cases.

## B.4 Document classification

In this experiment, we set the number of slices  $n_s = 20$  for SW,  $n_s = 10, T = 7, \kappa = 4$  for TSW. Numerical results are summarized in Table 3. We observed that PRHCP leads to the best

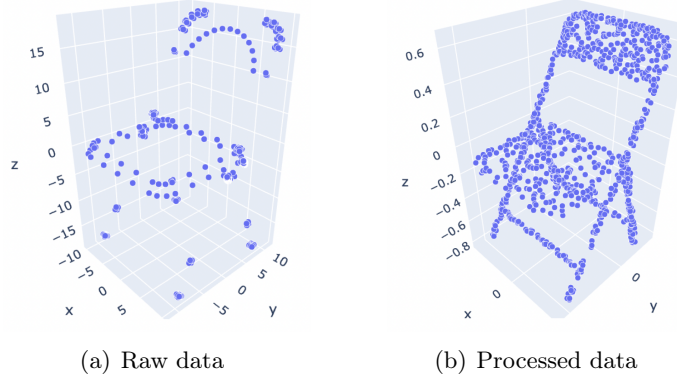


Figure 11: 3D point cloud preprocessing

Table 2: Comparisons on 3D point cloud classification

Method	Accuracy(%)					CPU time(s)				
	n=100	n=200	n=500	n=1000	n=2000	n=100	n=200	n=500	n=1000	n=2000
HCP	73.3 $\pm$ 1.3	79.2 $\pm$ 2.8	<b>81.8</b> $\pm$ 0.2	<b>81.0</b> $\pm$ 0.1	<b>82.3</b> $\pm$ 0.7	<b>17.9</b>	<b>34.3</b>	<b>90.4</b>	<b>186.7</b>	374.5
SW	71.5 $\pm$ 2.2	77.0 $\pm$ 1.0	79.2 $\pm$ 0.5	79.3 $\pm$ 0.7	80.5 $\pm$ 1.0	123.9	202.1	410.5	830.8	1808.7
TSW	72.7 $\pm$ 3.2	75.0 $\pm$ 2.5	77.0 $\pm$ 2.2	77.7 $\pm$ 1.5	78.0 $\pm$ 1.0	120.7	137.4	165.8	217.2	<b>282.1</b>
GSW(Poly5)	68.3 $\pm$ 2.0	73.2 $\pm$ 0.5	76.0 $\pm$ 0.7	76.8 $\pm$ 1.2	77.7 $\pm$ 0.3	839.7	940.6	1228.8	1782.4	2970.2
MMD	66.8 $\pm$ 4.2	71.8 $\pm$ 0.2	74.0 $\pm$ 0.7	/	/	153.6	385.7	1785.2	/	/
Sinkhorn	<b>77.0</b> $\pm$ 2.7	<b>80.8</b> $\pm$ 0.5	81.5 $\pm$ 0.8	/	/	768.7	2305.0	6184.6	/	/

performance, requiring reasonable CPU time.

## B.5 HCP-based auto-encoders

For the first implementation on low dimensional latent space, we used a simple autoencoder with mirrored classic deep convolutional neural networks with 2D average poolings, Leaky-ReLu activation functions, and upsampling layers in the decoder. The batch size is 500 and the number of projections for SWAE is 50. To evaluate the performance, we randomly selected a sample of size 1000 from the encoded test data points (blue points in Fig. 12(b)) and calculated the SW distance between this sample and a random sample from the target distribution in the latent space (red points in Fig. 12(b)). The SW distances versus the number of epochs w.r.t. the image space and the latent space are shown in Fig. 12(a). We observed that though these three methods perform similarly in the image space, our HCP-AE converges much faster in the latent space.

Figure 12(c) visualizes the samples from three different target distributions in the latent space, the encoded data samples via HCP-AE, and their generated images. We observed that the encoded samples capture the target distribution in the latent space effectively and are able to generate high

Table 3: Comparisons on document classification

Method	Accuracy	CPU time(s)
PRHCP	<b>74.6</b> $\pm$ 0.9	669.7
TSW	71.2 $\pm$ 0.6	<b>287.7</b>
Sinkhorn	70.0 $\pm$ 0.4	10106.7
SW	68.6 $\pm$ 1.1	2789.7

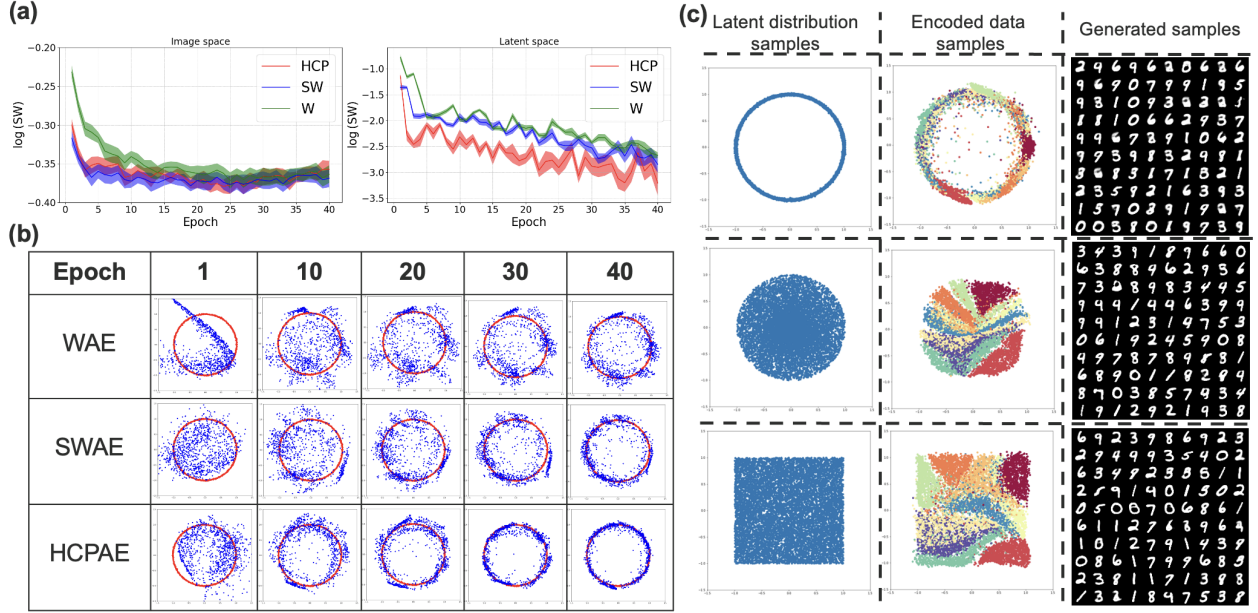


Figure 12: (a): SW distances between the target sample and the encoded testing sample w.r.t. the image space (left) and the latent space (right); (b) Visualization of these two sample in the latent space during training; (c) Visualization of the encoded samples and the generated images w.r.t. HCP-AE.

quality digital images.

For the second implement on high dimensional latent space, all the autoencoders have the same DCGAN-style architecture [36] and are learned with the same hyperparameters: the learning rate is 0.001; the optimizer is Adam [18] with  $\beta_1 = 0.9$  and  $\beta_2 = 0.999$ ; the number of epochs is 50; the batch size is 100; the weight of regularizer  $\gamma$  is 1; the dimension of latent code is 8 for MNIST and 64 for CelebA; the number of random projections is 50. All the autoencoders use Euclidean distance as the distance between samples, which means the reconstruction loss is the mean-square-error (MSE). Figure 19 shows more results for the linear interpolation between images and randomly generated images w.r.t. the proposed auto-encoders.

## C Additional analysis

### C.1 Why SW and its invariants converge slower than HCP in some cases?

Considering the experiment of approximation of Wasserstein flow, we observe that using SW or its invariants as the loss function may lead to slow convergence. We now provide an intuitive explanation for this observation using the *25-Gaussians* distribution as an example. We illustrate the iterations of SW, Max-SW, GSW, Max-GSW and HCP in Fig. 13. We observe that the flow w.r.t. SW and its variants go through 2 processes: firstly, red points spread out without covering the central Gaussian; secondly, they cover the central Gaussian slowly. Such an observation indicates linear projection fails to preserve high-dimensional data structure, especially when the data are multi-modal, and thus resulting in slow convergence. The proposed HCP distance utilizes Hilbert curve to preserve high-dimensional data structural and thus leads to faster convergence.



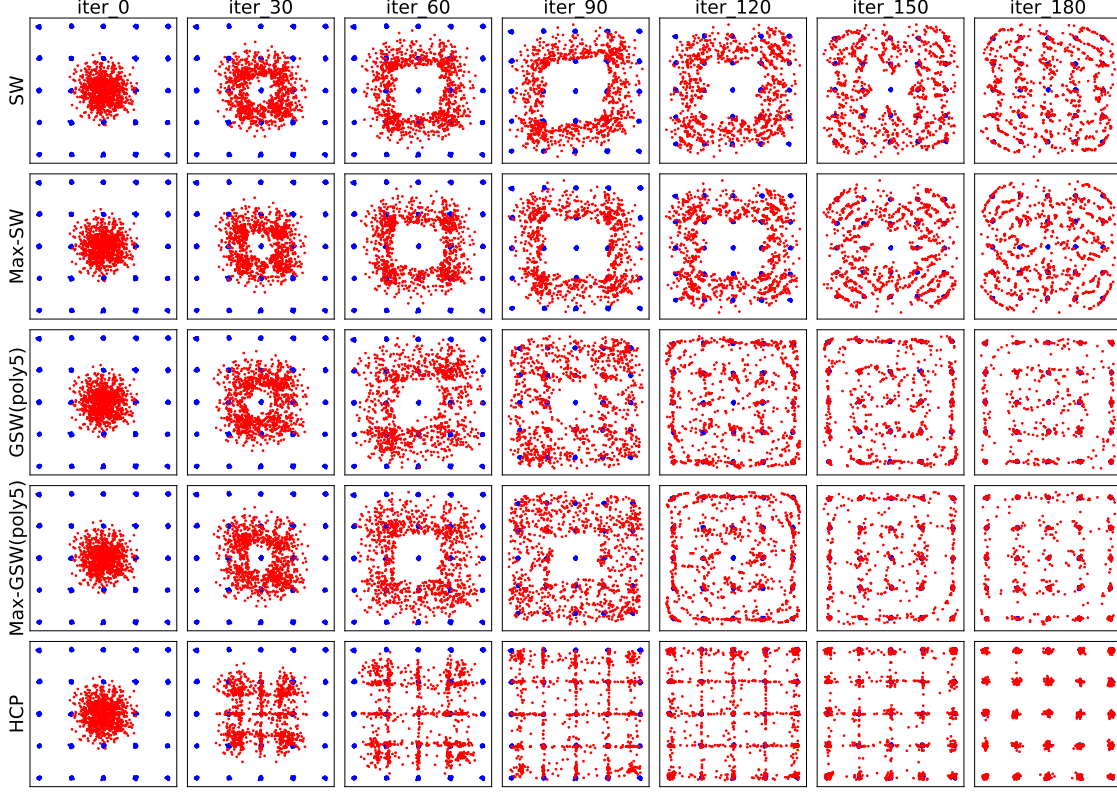


Figure 13: Iterations of different distances based flow.

## C.2 Robustness of PRHCP

Following the settings in [25; 32], we consider uniform distribution  $\mu = \mathcal{U}([-1, 1])^d$  and  $\nu = T_{\#}\mu$  the pushforward of  $\mu$  under the map  $T(x) = x + 2 \text{sign}(x) \odot \left( \sum_{i=1}^{q^*} e_i \right)$ , where  $\text{sign}$  is taken elementwise,  $q^* = 2, 4, 7, 10$  and  $(e_1, \dots, e_d)$  is the canonical basis of  $\mathbb{R}^d$ . The map  $T$  splits the hypercube into four different hyper-rectangles. This is to say, the dimension of the effective subspace equals  $q^*$ . Figure 14 shows the PRHCP distance increases rapidly when  $q < q^*$  and increases slowly when  $q > q^*$ . Such an observation indicates PRHCP can dig out useful subspace information effectively.

## C.3 Empirical sample complexity

We consider a synthetic example to demonstrate the empirical sample complexity of the proposed distances. We generate two samples of size  $n$  from the standard  $d$ -dimensional Gaussian distributions and we calculate the distances between these two samples w.r.t. different distance metrics. Figure 15 shows the average distances w.r.t. 100 replications versus  $n$  for  $d = 2$  (left) and  $d = 20$  (right), respectively. We observe that when  $d = 20$ , the Wasserstein distance and the HCP distance converge slowly as expected, while

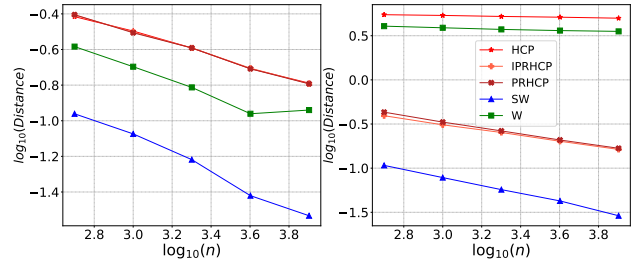


Figure 15: Comparison for sample complexity. Left:  $d = 2$ . Right:  $d = 20$ . Each curve represents the average distance w.r.t. 100 replications.

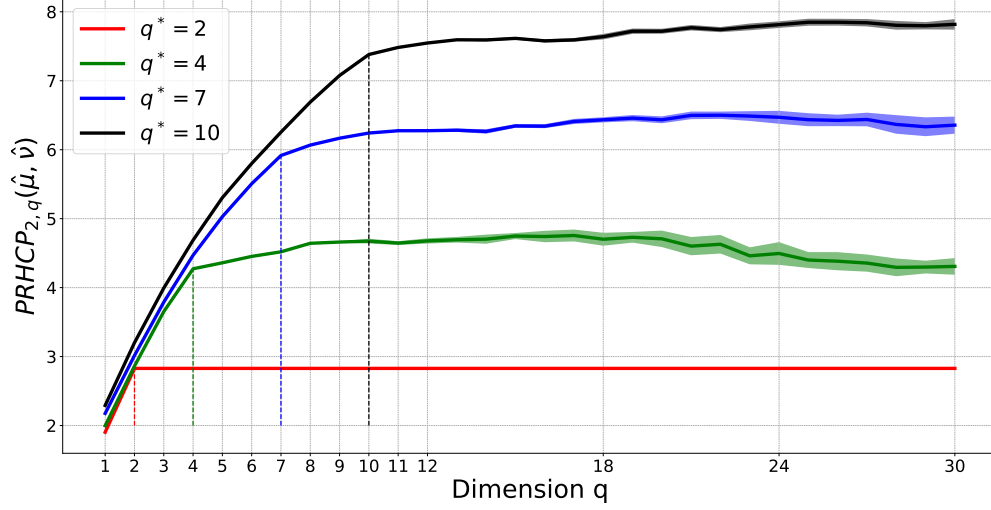


Figure 14:  $\text{PRHCP}_{2,q}(\mu_n, \nu_n)$  versus the dimension  $q$  for  $q^* = 2, 4, 7, 10$ . Each curve is the mean of 100 replications.

SW, IPRHCP and PRHCP converge much faster.

#### C.4 Effect of the order $k$

We analyze the effect of  $k$  in the proposed HCP distance using a synthetic example. We generate two samples of size  $n$  from the uniform distribution on the unit hypercube  $[0, 1]^d$  and we calculate the HCP distance between these two samples. All the experiments are replicated 100 times. The left panel of Fig. 16 shows the average HCP distances versus different  $n$ , and the right panel of which shows the average CPU time for generating the  $k$ -order Hilbert curve when  $d = 2$ . The results for  $d = 10$  are shown in Fig. 17. From these two figures, we observe that the HCP distance is not sensitive to the choice of  $k$ , as long as  $k$  is not too small. We also observe that the computational cost for generating the  $k$ -order Hilbert curve is linear to  $n$ . In addition, the results in Fig. 18 indicate the computational cost for generating the  $k$ -order Hilbert curve is linear to  $d$ .

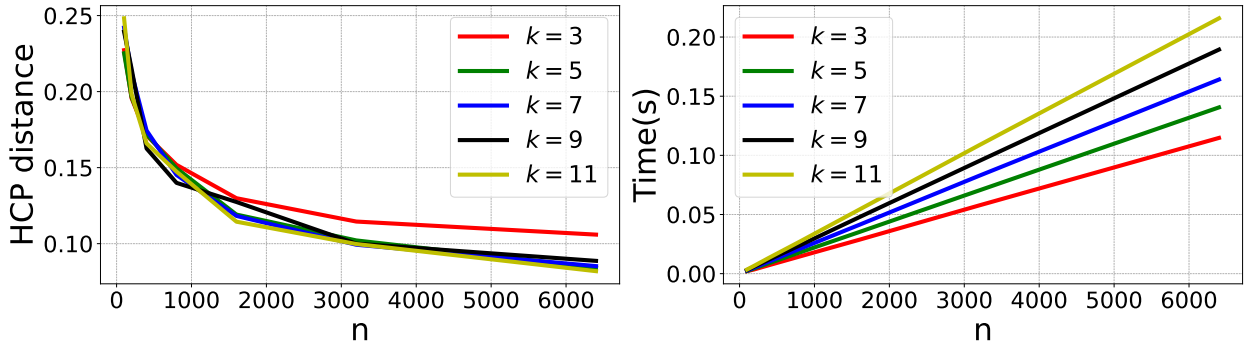


Figure 16: Left: HCP distance versus  $n$  when  $d = 2$ . Right: CPU time for generating the  $k$ -order Hilbert curve versus  $n$  when  $d = 2$ . Each curve represents the average of 100 replications.

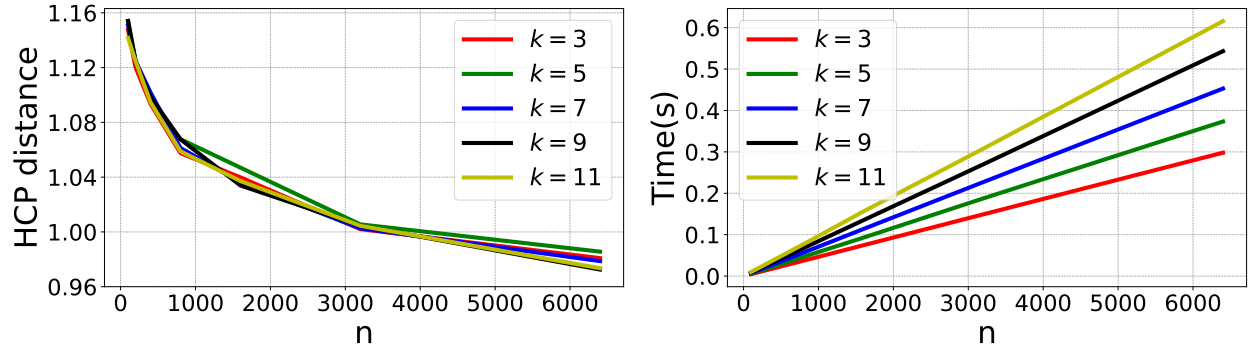


Figure 17: Left: HCP distance versus  $n$  when  $d = 10$ . Right: CPU time for generating the  $k$ -order Hilbert curve versus  $n$  when  $d = 10$ . Each curve represents the average of 100 replications.

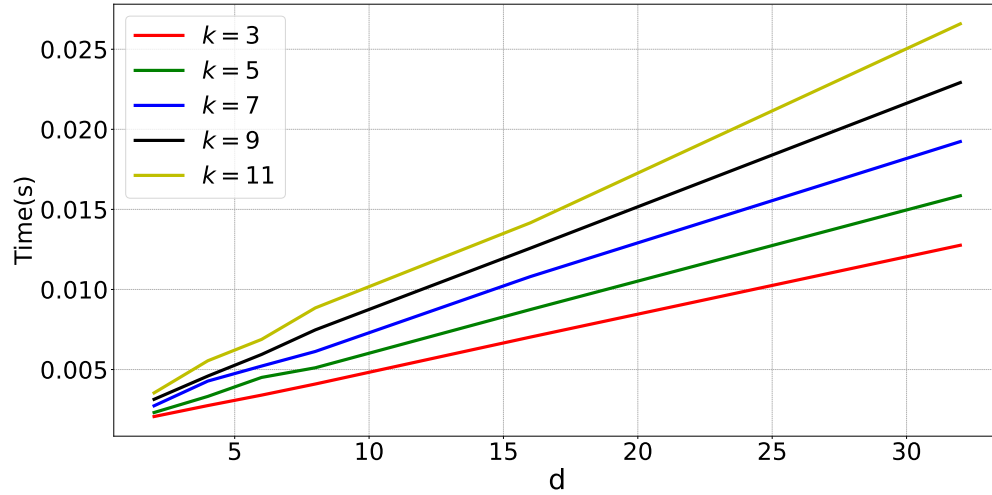


Figure 18: CPU time for generating the  $k$ -order Hilbert curve versus  $d$  when  $n = 100$ . Each curve represents the average of 100 replications



(a) IPRHCP-AE



(b) PRHCP-AE

Figure 19: The performance of our generators on face generation and interpolation.